Secure Wireless Communication in Active RIS-Assisted DFRC Systems

Yang Zhang [ID], Hong Ren [ID], *Member, IEEE*, Cunhua Pan [ID], *Senior Member, IEEE*, Boshi Wang, Zhiyuan Yu [ID], Ruisong Weng [ID], Tuo Wu [ID], and Yongchao He

Abstract—This work considers a dual-functional radar and communication (DFRC) system with an active reconfigurable intelligent surface (RIS) and a potential eavesdropper. Our purpose is to maximize the secrecy rate (SR) of the system by jointly designing the beamforming matrix at the DFRC base station (BS) and the reflecting coefficients at the active RIS, subject to the signal-to-interference-plus-noise-ratio (SINR) constraint of the radar echo and the power consumption constraints at the DFRC-BS and active RIS. An alternating optimization (AO) algorithm based on semidefinite relaxation (SDR) and majorization-minimization (MM) is applied to solve the SR-maximization problem by alternately optimizing the beamforming matrix and the reflecting coefficients. Specifically, we first apply the SDR and successive convex approximation (SCA) methods to transform the two subproblems into more tractable forms, then the MM method is applied to derive a concave surrogate function and iteratively solve the subproblems. Finally, simulation results indicate that the active RIS can better confront the impact of "multiplicative fading" and outperforms traditional passive RIS in terms of both secure data rate and radar sensing performance.

Index Terms—Reconfigurable intelligent surface (RIS), integrated sensing and communication (ISAC), dual-functional radar and communication (DFRC), physical layer security (PLS), active RIS.

I. INTRODUCTION

INTEGRATED sensing and communication (ISAC) has attracted increasing attention in recent years as one of the key candidate technologies to provide high-quality wireless communication and radar sensing function. However, the sensing function requires extra bandwidth and thereby intensifies the problem of spectrum congestion. As a promising solution, the dual-functional radar and communication (DFRC) is regarded as the paradigm of ISAC network for its resource efficiency, which is capable of realizing communication and radar spectrum sharing (CRSS) as well as the shared use of hardware platform [1], [2], [3], [4], [5].

However, the dual-functional nature of DFRC signal may lead to serious security concerns which is often ignored in relevant studies. It is noteworthy that the DFRC transmit signal is a jointly-designed waveform carrying both communication and sensing signals. Hence, the embedded data can be easily leaked to potential eavesdroppers and even targets when there is no specific design to deal with the security issue. There have been several studies in secure wireless communication in DFRC systems recently [6], [7], [8], [9]. In particular, the authors of [8], [9] considered the scenario where the targets serve as the potential eavesdroppers in the multiple-input multiple-output (MIMO) DFRC system, and proposed various algorithms for the cases of imperfect, statistical channel state information (CSI), and uncertain target direction estimation. Nevertheless, when the channel of the legitimate communication user and that of the potential eavesdropper are highly correlated, the aforementioned techniques face limitations in terms of secrecy rate (SR).

The reconfigurable intelligent surface (RIS) can be an effective solution to the aforementioned problems owing to its capacity of manipulating the wireless environment. Specifically, an RIS is a meta-surface consisting of various low-cost passive reflecting elements, each of which is capable of controlling the phase shift of the incident signal independently. For communication tasks, the RIS can establish virtual links and reconfigure the reflected signals constructively for legitimate users and destructively for eavesdroppers by controlling the elements. Consequently, it can strengthen the quality of service (QoS) of legitimate users and weaken that of eavesdroppers, and thus enhance the secure communication performance of the DFRC system [10], [11], [12], [13], [14], [15]. For sensing tasks, the deployment of RIS can create a virtual line-of-sight (LoS) link for the sensing targets located in the non-line-of-sight (NLoS) area of the DFRC base station (BS) and solve the problem that the millimeter wave (MMW) can be easily obstructed. Therefore, the deployment of RIS is regarded as an appealing innovation in ISAC systems. Thanks to the above-mentioned advantages of the RIS, RIS-assisted DFRC systems have been well studied over the past few years [2], [16], [17], [18], [19], [20], [21], [22]. Generally, transmit beamforming vectors and the RIS coefficients are jointly optimized in these studies for desired performance gain in

Yang Zhang, Hong Ren, Cunhua Pan, Boshi Wang, Zhiyuan Yu, Ruisong Weng, and Yongchao He are with the National Mobile Communications Research Laboratory, Southeast University, Nanjing 210096, China (e-mail: 220230982@seu.edu.cn; hren@seu.edu.cn; cpan@seu.edu.cn; 220230800@seu.edu.cn; zyyu@seu.edu.cn; 230239439@seu.edu.cn; heyongchao@seu.edu.cn).

Tuo Wu is with the School of Electronic Engineering and Computer Science, Queen Mary University of London, E1 4NS London, U.K. (e-mail: tuo.wu@qmul.ac.uk).

communication or radar sensing. In particular, the authors of [16] considered the four-hop echo model which is more practical in RIS-assisted DFRC systems and proposed some methods to tackle the quartic expression of the four-hop radar SINR without considering the security problem. In addition, the authors of [20] considered the dual-functional performance of an RIS-assisted secure ISAC system, where the RIS not only enhances the secrecy performance but also creates a virtual LoS link for the target. Nevertheless, the secrecy performance is evaluated by the SINR at the users and the eavesdropper instead of the SR of the system.

Nevertheless, the performance gain of these passive RIS-assisted schemes is limited owing to the "multiplicative fading" effect of the RIS-reflecting link. In particular, the path loss of the multi-hop link is equivalent to the product of those of the constituent channels. As demonstrated in previous works, the capacity gain provided by the RIS-reflecting channel can only be observed when the direct link is very weak, which is owing to the severe equivalent path loss of the RIS-reflecting channel [23]. This may result in limited QoS at legitimate users and low received signal power at the BS, limiting the dual-functional performance of the system. Although passive RIS can provide an array gain proportional to square of the number of its elements [24], [25], it requires a large number of reflecting elements to overcome the severe propagation loss, which will result in high channel estimation overhead and excessive optimization complexity [26], [27].

To overcome the "multiplicative fading" effect in passive RIS-assisted systems, the novel concept of active RIS has been proposed recently [23]. In particular, each element of the active RIS is equipped with a reflection-type amplifier, so the amplitude and phase shift of the reflected signal can be adjusted simultaneously with extra power consumption and non-negligible thermal noise. Based on the amplification function, the active RIS can efficiently address the severe fading issue and acquire higher received signal power through the RIS-reflecting channel compared with the traditional passive RIS [28], [29]. In terms of the security of wireless networks, the active RIS can achieve much better QoS of legitimate users, while destructively reconfiguring the signals to the eavesdroppers for less data leakage. Hence, active RISs have been recently amalgamated with physical layer security. For example, the authors of [30] and [31] have proposed a novel scheme of active RIS-assisted secure communication in a multiple-input single-output (MISO) system, and presented solutions to several optimization problems including SR maximization. Furthermore, the authors of [32] proposed a novel framework of double-faced active RIS to enhance the secure communication performance. However, these works are restricted to non-sensing settings and their algorithms cannot be applied straightforward to the DFRC models.

Owing to the aforementioned research gaps, the deployment of the active RIS is also regarded as a promising innovation in secure DFRC systems. Except for the advantages in security concerns, it is also demonstrated that the active RIS is suitable to overcome the severe propagation loss of the multi-hop radar echo channel, and obtain higher signal power at the receiver of the DFRC-BS for better sensing resolution [33], [34], [35].

However, there are only a few contributions devoted to the security problem in active RIS-assisted DFRC systems. In particular, the authors of [36] studied the secure communication in an active RIS-assisted THz ISAC system with delay alignment modulation, while the dedicated sensing signal is not considered in their system model, and the four-hop radar echo is not appplied as the sensing metric. In addition, the authors of [37] studied the SR maximization problem in an active RIS-assisted mutiple-user multiple-input single-output (MU-MISO) DFRC system by jointly designing the transmit beamformers, the radar receive beamformers and the reflecting coefficient matrix at the active RIS. They also considered the four-hop radar SINR to evaluate the sensing function of the DFRC system. However, the thermal noise introduced by the active RIS, the interference in the radar echo, and extra power consumption were totally neglected in their system model, which is an ideal assumption ignoring the practical features of the active RIS.

Motivated by the aforementioned background, this paper aims at investigating the SR maximization problem in an MISO DFRC system with the presence of active eavesdropping. In particular, the non-negligible interference and noise in the four-hop radar echo signal and extra power consumption at the active RIS are considered. The main contributions of this paper are summarized as follows:

1) We consider an active RIS-assisted DFRC system with a DFRC-BS, a single-antenna legitimate user and a potential eavesdropper as well as a target located in the NLoS area of the BS. Then, we formulate an SR maximization problem subject to the transmit power budget and radar SINR constraints, and optimize the BS precoding matrix and the RIS reflecting coefficients.

2) We propose an alternating optimization (AO) algorithm based on the semi-definite relaxation (SDR) and majorization-minimization (MM) algorithm to tackle the non-convex problem. In each subproblem decomposed by the AO algorithm, we first use the method of successive convex approximation (SCA) to handle the radar SINR constraint and apply SDR to reformulate the problem. Then we obtain the concave approximation function by using the first-order Taylor expansion, and apply the MM algorithm to iteratively solve the subproblems. By alternately optimizing the precoding matrix and the reflecting coefficients, the algorithm can converge to a sub-optimal point of the original problem.

3) Simulation results are presented to verify the advantages of the active RISs over traditional passive RISs with the same total power budget in our proposed scenario. It is demonstrated that both the SR and the radar SINR of the DFRC system can be significantly enhanced with the deployment of an active RIS. Besides, the results indicate that the SR performance can be enhanced by increasing the transmit power and the number of RIS elements, and the power allocation between the DFRC-BS and the active RIS also has significant impact on the achievable SR.

The remainder of this paper is organized as follows. In Section II, we introduce the system model of the active RIS-assisted DFRC system, and formulate the SR maximization
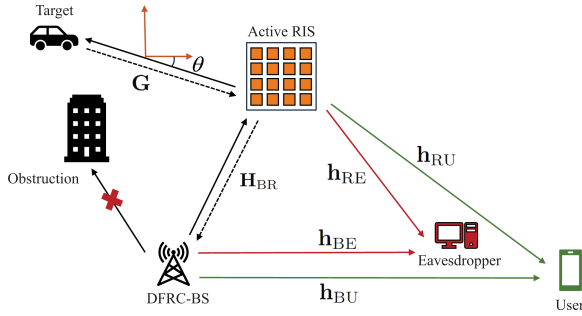
Fig. 1.   An active RIS-assisted secure DFRC system.

problem. In Section III, we develop an SDR-MM-based algorithm. Simulation results are provided in Section IV, and Section V briefly concludes the paper.

Notations: Constants, vectors and matrices are denoted by italics, boldface lowercase and boldface uppercase letters, respectively. For a complex value a, $\mathrm{Re}(a)$ denotes the real part of a. For a real value b, $[b]^+$ denotes $\max(b, 0)$. $\mathbb{C}^{M \times N}$ denotes the set of $M \times N$ complex vectors or matrices. $\mathbb{E}\{\cdot\}$ denotes the expectation operation. $\|\mathbf{x}\|_2$ denotes the 2-norm of vector $\mathbf{x}$. $\|\mathbf{A}\|_{\mathrm{F}}$ and $\mathrm{tr}(\mathbf{A})$ denote the Frobenius norm and trace of $\mathbf{A}$, respectively. $\mathbf{A}^*$, $\mathbf{A}^{\mathrm{T}}$ and $\mathbf{A}^{\mathrm{H}}$ denote the conjugate, transpose and Hermitian transpose of $\mathbf{A}$, respectively. $\mathbf{A}_{[m,n]}$ denotes the (m, n)-th entry of $\mathbf{A}$. $\mathrm{diag}(\cdot)$ and $\mathrm{vec}(\cdot)$ represent the diagonalization and vectorization operators, respectively. $\Sigma(\mathbf{x})$ denotes the operator of transforming vector $\mathbf{x} \in \mathbb{C}^{N^2 \times 1}$ into an $N \times N$ matrix. $\nabla f(\mathbf{x})$ denotes the gradient of the function f with respect to (w.r.t.) the vector $\mathbf{x}$. $\mathbf{B} \otimes \mathbf{C}$ denotes the Kronecker product of $\mathbf{B}$ and $\mathbf{C}$. $\mathbf{I}_N$ denotes the $N \times N$ identity matrix, and $\mathbf{r} \sim \mathcal{CN}(\mathbf{0}, \mathbf{I})$ denotes a random vector following the Gaussian distribution of zero mean and unit variance.

II. SYSTEM MODEL AND PROBLEM FORMULATION

A. System Model

As shown in Fig. 1, we consider an active RIS-assisted secure DFRC system. The DFRC-BS equipped with a uniform linear array (ULA) of M antennas serves a single-antenna legitimate user, while a single-antenna eavesdropper intends to wiretap the confidential information. Meanwhile, the DFRC-BS also intends to detect a point-like target, which is located at the NLoS area of the DFRC-BS.[1] Besides, an active RIS with N reflecting elements is deployed in the system to assist the radar sensing and secure communication.

1) Transmit Signal Model: We consider that the BS sends both confidential communication and dedicated sensing signals using transmit beamforming technique to facilitate the dual function of the system. Let us denote s as the confidential communication signal and $\mathbf{d} \in \mathbb{C}^{M \times 1}$ as the dedicated sensing

---

[1]We adopt this assumption to lay emphasis on the function of the RIS in creating virtual LoS link for sensing function. If the direct link between the DFRC-BS and the target is not negligible, the expression of the radar echo can be more complicated and challenging to handle. Nevertheless, our algorithm can still be applicable to the aforementioned scenario owing to the identical key challenges, such as the quartic form of the radar SINR constraint.

signal, respectively. It is assumed that the dedicated sensing signal $\mathbf{d}$ is generated as pseudo-random sequences satisfying $\mathbb{E}\{\mathbf{d}\} = \mathbf{0}$ and $\mathbb{E}\{\mathbf{d}\mathbf{d}^{\mathrm{H}}\} = \mathbf{I}_M$, and can be *a priori* known by the DFRC-BS, the user and the eavesdropper [38]. In addition, the communication signal satisfies $s \sim \mathcal{CN}(0, 1)$, and is independent of the dedicated sensing signal. We denote $\mathbf{W}_{\mathrm{r}} \triangleq [\mathbf{w}_{\mathrm{r},1}, \mathbf{w}_{\mathrm{r},2}, \dots, \mathbf{w}_{\mathrm{r},M}] \in \mathbb{C}^{M \times M}$ and $\mathbf{w}_{\mathrm{c}} \in \mathbb{C}^{M \times 1}$ as the beamforming matrix and vector of sensing and communication signals, respectively. Therefore, the transmit signal of the DFRC-BS is given by

$$\mathbf{x} = \mathbf{W}_{\mathrm{r}}\mathbf{d} + \mathbf{w}_{\mathrm{c}}s \triangleq \mathbf{W}\hat{\mathbf{s}}, \tag{1}$$

where $\mathbf{W} \triangleq [\mathbf{W}_{\mathrm{r}}, \mathbf{w}_{\mathrm{c}}] \in \mathbb{C}^{M \times (M+1)}$, $\hat{\mathbf{s}} \triangleq [\mathbf{d}^{\mathrm{T}}, s]^{\mathrm{T}} \in \mathbb{C}^{(M+1) \times 1}$, and the covariance matrix of the transmit signal can be written as

$$\mathbf{R} = \mathbb{E}\{\mathbf{x}\mathbf{x}^{\mathrm{H}}\} = \mathbf{W}\mathbf{W}^{\mathrm{H}} = \sum_{i=1}^{M+1} \mathbf{w}_i \mathbf{w}_i^{\mathrm{H}}, \tag{2}$$

where $\mathbf{w}_i$ denotes the i-th column of matrix $\mathbf{W}$.

We first consider the secure communication function and denote $\mathbf{H}_{\mathrm{BR}} \in \mathbb{C}^{N \times M}$, $\mathbf{h}_{\mathrm{BU}} \in \mathbb{C}^{M \times 1}$, $\mathbf{h}_{\mathrm{BE}} \in \mathbb{C}^{M \times 1}$, $\mathbf{h}_{\mathrm{RU}} \in \mathbb{C}^{N \times 1}$, and $\mathbf{h}_{\mathrm{RE}} \in \mathbb{C}^{N \times 1}$ as the channel coefficients from the BS to the RIS, from the BS to the user, from the BS to the eavesdropper, from the RIS to the user and from the RIS to the eavesdropper, respectively. We also assume that the CSI of the above channels is perfectly known at the DFRC-BS by applying low-complexity channel estimation methods [39], [40], [41]. It is worth noting that the eavesdropper is assumed to wiretap the communication signal by actively attacking the system. Specifically, the eavesdropper can mislead the DFRC-BS by sending pilot signals during the channel estimation phase and pretend to be a legitimate user [42]. Therefore, the DFRC-BS can acquire the CSI of both the user and the eavesdropper during the channel estimation procedure. Furthermore, owing to the severe multiplicative path loss, we can neglect the signals reflected by the active RIS for more than two times. Therefore, the signal received at the legitimate user and the eavesdropper can be respectively given by

$$y_{\mathrm{U}} = \left(\mathbf{h}_{\mathrm{BU}}^{\mathrm{H}} + \mathbf{h}_{\mathrm{RU}}^{\mathrm{H}}\boldsymbol{\Phi}\mathbf{H}_{\mathrm{BR}}\right)\mathbf{x} + \mathbf{h}_{\mathrm{RU}}^{\mathrm{H}}\boldsymbol{\Phi}\mathbf{v}_1 + n_{\mathrm{U}}, \tag{3}$$

$$y_{\mathrm{E}} = \left(\mathbf{h}_{\mathrm{BE}}^{\mathrm{H}} + \mathbf{h}_{\mathrm{RE}}^{\mathrm{H}}\boldsymbol{\Phi}\mathbf{H}_{\mathrm{BR}}\right)\mathbf{x} + \mathbf{h}_{\mathrm{RE}}^{\mathrm{H}}\boldsymbol{\Phi}\mathbf{v}_1 + n_{\mathrm{E}}, \tag{4}$$

where $n_{\mathrm{U}} \sim \mathcal{CN}(0, \sigma_{\mathrm{U}}^2)$ and $n_{\mathrm{E}} \sim \mathcal{CN}(0, \sigma_{\mathrm{E}}^2)$ denote the additive white Gaussian noise (AWGN) at the user and eavesdropper, respectively, and matrix $\boldsymbol{\Phi} = \mathrm{diag}(\phi_1, \phi_2, \dots, \phi_N)$ is the diagonal reflecting coefficient matrix of the active RIS with $\phi_i = \beta_i e^{j\vartheta_i}$, where $\beta_i \geq 0$ and $\vartheta_i \in [0, 2\pi)$ are the amplitude and the phase shift of the i-th reflecting element, respectively. Compared with traditional passive RISs, the elements of an active RIS are equipped with reflection-type amplifiers which consume extra power to amplify the incident signal, and thus the thermal noise at the active RIS is non-negligible. Furthermore, the amplitude β_i also represents the amplification gain of the i-th reflecting element, and satisfies $\beta_i \leq \eta_i$ with $\eta_i > 1$ denoting the maximum amplification gain. Finally, the vector $\mathbf{v}_1 \sim \mathcal{CN}(\mathbf{0}, \sigma_{v_1}^2 \mathbf{I}_N)$ denotes the zero-mean AWGN at the active RIS.

Then, we consider the sensing function of the DFRC system. We assume that the potential target is located in the NLoS area of the BS owing to the blockage, and the virtual LoS channel created by the active RIS is much stronger than the NLoS one. Hence, the effect of NLoS channel between the BS and sensing target can be neglected. In addition, it is assumed that the location of the active RIS is well designed with few obstacles. Therefore, we define the response channel matrix $\mathbf{G} \in \mathbb{C}^{N \times N}$ of the sensing target to the RIS as

$$\mathbf{G} = \gamma \mathbf{a}(\theta) \mathbf{a}^{\mathrm{H}}(\theta), \quad (5)$$

which is based on the clutter-free model [43], [44], and γ denotes the complex path loss coefficient of the response channel. The vector $\mathbf{a}(\theta)$ represents the steering vector of the RIS and θ denotes the angle of departure (AoD) of the target towards the active RIS, which is given by

$$\mathbf{a}(\theta) = \left[1, e^{j2\pi \frac{d_{\mathrm{RIS}}}{\lambda} \sin\theta}, \ldots, e^{j2\pi \frac{d_{\mathrm{RIS}}}{\lambda}(N-1)\sin\theta}\right]^{\mathrm{H}}, \quad (6)$$

where d_{RIS} denotes the interval between adjacent RIS elements and λ denotes the carrier wavelength. Since the information signal s and the dedicated sensing signal $\mathbf{d}$ can be jointly utilized to illuminate the sensing target, the radar echo received at the DFRC-BS can be given as

$$\mathbf{y}_{\mathrm{R}} = \mathbf{H}_{\mathrm{BR}}^{\mathrm{H}} \mathbf{\Phi}^{\mathrm{H}} \mathbf{G} \mathbf{\Phi} \mathbf{H}_{\mathrm{BR}} \mathbf{x} + \mathbf{H}_{\mathrm{BR}}^{\mathrm{H}} \mathbf{\Phi}^{\mathrm{H}} \mathbf{G} \mathbf{\Phi} \mathbf{v}_1$$
$$+ \mathbf{H}_{\mathrm{BR}}^{\mathrm{H}} \mathbf{\Phi} \mathbf{v}_1 + \mathbf{H}_{\mathrm{BR}}^{\mathrm{H}} \mathbf{\Phi}^{\mathrm{H}} \mathbf{v}_2 + \underbrace{\mathbf{H}_{\mathrm{BR}}^{\mathrm{H}} \mathbf{\Phi} \mathbf{H}_{\mathrm{BR}} \mathbf{x}}_{\text{Interference Echo}} + \mathbf{n}_{\mathrm{R}}, \quad (7)$$

where the vectors $\mathbf{v}_2 \sim \mathcal{CN}(\mathbf{0}, \sigma_{v_2}^2 \mathbf{I}_N)$ and $\mathbf{n}_{\mathrm{R}} \sim \mathcal{CN}(\mathbf{0}, \sigma_{\mathrm{R}}^2 \mathbf{I}_M)$ denote the dynamic thermal noise at the active RIS in the uplink reflected signal and the noise at the DFRC-BS receiver, respectively. Note that the reflecting coefficients are considered as the same in the two reflections during the transmission, since the active RIS cannot switch its elements within the time interval between the two reflections.[2] In addition, the echo directly reflected by the RIS in the first reflection in (7), namely $\mathbf{H}_{\mathrm{BR}}^{\mathrm{H}} \mathbf{\Phi} \mathbf{H}_{\mathrm{BR}} \mathbf{x}$, is considered as interference with no information of the sensing target.

Finally, it is worth noting that the active RIS first reflects the transmit signal to the legitimate user, eavesdropper and the target, then reflects the echo signal from the target to the DFRC-BS. The first and second reflected signal in this process can be respectively given by

$$\mathbf{y}_{\mathrm{r}_1} = \mathbf{\Phi} \mathbf{H}_{\mathrm{BR}} \mathbf{x} + \mathbf{\Phi} \mathbf{v}_1, \quad (8)$$

$$\mathbf{y}_{\mathrm{r}_2} = \mathbf{\Phi}^{\mathrm{H}} \mathbf{G} \mathbf{\Phi} \mathbf{H}_{\mathrm{BR}} \mathbf{x} + \mathbf{\Phi}^{\mathrm{H}} \mathbf{G} \mathbf{\Phi} \mathbf{v}_1 + \mathbf{\Phi}^{\mathrm{H}} \mathbf{v}_2. \quad (9)$$

2) Metrics of Dual Functional Performance: Firstly, based on the aforementioned model of transmit signal, the signal-to-noise-ratio (SNR) of the legitimate user and the eavesdropper

are respectively give as

$$\xi_{\mathrm{U}} = \frac{\left|\left(\mathbf{h}_{\mathrm{BU}}^{\mathrm{H}} + \mathbf{h}_{\mathrm{RU}}^{\mathrm{H}} \mathbf{\Phi} \mathbf{H}_{\mathrm{BR}}\right) \mathbf{w}_{\mathrm{c}}\right|^2}{\sigma_{v_1}^2 \left\|\mathbf{h}_{\mathrm{RU}}^{\mathrm{H}} \mathbf{\Phi}\right\|_2^2 + \sigma_{\mathrm{U}}^2}, \quad (10)$$

$$\xi_{\mathrm{E}} = \frac{\left|\left(\mathbf{h}_{\mathrm{BE}}^{\mathrm{H}} + \mathbf{h}_{\mathrm{RE}}^{\mathrm{H}} \mathbf{\Phi} \mathbf{H}_{\mathrm{BR}}\right) \mathbf{w}_{\mathrm{c}}\right|^2}{\sigma_{v_1}^2 \left\|\mathbf{h}_{\mathrm{RE}}^{\mathrm{H}} \mathbf{\Phi}\right\|_2^2 + \sigma_{\mathrm{E}}^2}. \quad (11)$$

Note that the user and the eavesdropper are assumed to be capable of canceling the sensing interference with the prior knowledge of the dedicated sensing signal[3]. In addition, the dedicated sensing signal $\mathbf{d}$ is generated as pseudo-random sequences and readily known by the user and the eavesdropper prior to the transmission. Hence, both the legitimate user and the eavesdropper are capable of canceling the sensing interference with the prior knowledge of $\mathbf{d}$ via interference cancellation techniques such as successive interference cancellation [17], [45], [46]. Therefore, the achievable transmission rate (nat/s/Hz) of the user and eavesdropper can be respectively written as

$$R_{\mathrm{U}} = \ln(1 + \xi_{\mathrm{U}}), R_{\mathrm{E}} = \ln(1 + \xi_{\mathrm{E}}). \quad (12)$$

Then, the secrecy rate from the user to the DFRC-BS is given by

$$S = [R_{\mathrm{U}} - R_{\mathrm{E}}]^+. \quad (13)$$

For radar sensing function, it is worth noting that the DFRC-BS receiver has the complete knowledge of the transmit signal $\mathbf{x}$, so the communication waveform as well as the sensing signal in the radar echo can be utilized. Let us define the following matrices

$$\mathbf{A} \triangleq \mathbf{H}_{\mathrm{BR}}^{\mathrm{H}} \mathbf{\Phi}^{\mathrm{H}} \mathbf{G} \mathbf{\Phi} \mathbf{H}_{\mathrm{BR}}, \mathbf{B} \triangleq \mathbf{H}_{\mathrm{BR}}^{\mathrm{H}} \mathbf{\Phi} \mathbf{H}_{\mathrm{BR}},$$

$$\mathbf{C} \triangleq \mathbf{H}_{\mathrm{BR}}^{\mathrm{H}} \mathbf{\Phi}^{\mathrm{H}} \mathbf{G} \mathbf{\Phi} + \mathbf{H}_{\mathrm{BR}}^{\mathrm{H}} \mathbf{\Phi}, \mathbf{D} \triangleq \mathbf{H}_{\mathrm{BR}}^{\mathrm{H}} \mathbf{\Phi}^{\mathrm{H}},$$

then the SINR of radar echo received at the DFRC-BS receiver can be written as [19], [47]

$$\xi_{\mathrm{R}} = \mathrm{tr}\left(\mathbf{A} \mathbf{R} \mathbf{A}^{\mathrm{H}} \mathbf{J}^{-1}\right), \quad (14)$$

where $\mathbf{J}$ represents the interference-plus-noise covariance matrix, which is given by [48]

$$\mathbf{J} = \mathbf{B} \mathbf{R} \mathbf{B}^{\mathrm{H}} + \mathbf{N}, \quad (15)$$

where

$$\mathbf{N} = \sigma_{v_1}^2 \mathbf{C} \mathbf{C}^{\mathrm{H}} + \sigma_{v_2}^2 \mathbf{D} \mathbf{D}^{\mathrm{H}} + \sigma_{\mathrm{R}}^2 \mathbf{I}_M. \quad (16)$$

In addition, the transmit power of the DFRC-BS can be expressed as

$$P_{\mathrm{t}} = \mathbb{E}\left\{\|\mathbf{x}\|_2^2\right\} = \mathrm{tr}(\mathbf{R}), \quad (17)$$

---

[2]The technique of reconfiguring the RIS elements based on the positive-intrinsic-negative (PIN) diodes is widely applied in practical, and the minimum switching time of PIN diodes is $0.2\mu s$ [24]. Hence, owing to the severe path loss of the radar response channel, we assume that the distance between the active RIS and the target is not long enough for the RIS to switch its elements during the propagation interval.

[3]The authors of [45] have defined two types of communication receivers in ISAC systems as type-I and type-II receivers. In particular, type-I receivers are not capable of canceling the interference introduced by the dedicated sensing signal, while type-II receivers can cancel the interference with prior knowledge of the sensing signal. We assume that the legitimate user and the eavesdropper are both type-II receivers in this paper.

and the power consumption of the active RIS in the first and second reflection can be respectively given by

$$P_{A_1} = \mathbb{E}\left\{\|\mathbf{y}_{r_1}\|_2^2\right\}$$

$$= \text{tr}\left(\mathbf{H}_{BR}^H \boldsymbol{\Phi}^H \boldsymbol{\Phi} \mathbf{H}_{BR} \mathbf{R}\right) + \sigma_{v_1}^2 \|\boldsymbol{\Phi}\|_F^2,$$

$$P_{A_2} = \mathbb{E}\left\{\|\mathbf{y}_{r_2}\|_2^2\right\} \tag{18}$$

$$= \text{tr}\left(\mathbf{H}_{BR}^H \boldsymbol{\Phi}^H \mathbf{G}^H \boldsymbol{\Phi} \boldsymbol{\Phi}^H \mathbf{G} \boldsymbol{\Phi} \mathbf{H}_{BR} \mathbf{R}\right)$$

$$+ \sigma_{v_1}^2 \left\|\boldsymbol{\Phi}^H \mathbf{G} \boldsymbol{\Phi}\right\|_F^2 + \sigma_{v_2}^2 \|\boldsymbol{\Phi}\|_F^2. \tag{19}$$

B. Problem Formulation

In this paper, we aim to maximize the SR of the DFRC system by jointly optimizing the transmit beamforming matrix $\mathbf{W}$ at the DFRC-BS and the reflecting coefficient matrix $\boldsymbol{\Phi}$ at the active RIS, subject to the transmit power constraints at the DFRC-BS and the active RIS, the minimum radar SINR constraint and the maximum amplification gain constraint. Therefore, the SR maximization problem can be formulated as follows:

$$\max_{\mathbf{W},\boldsymbol{\Phi}} \quad R_U - R_E \tag{20a}$$

$$\text{s.t.} \quad \xi_R \geq \gamma_r, \tag{20b}$$

$$P_t \leq P_0, \tag{20c}$$

$$P_{A_1} + P_{A_2} \leq P_{RIS}, \tag{20d}$$

$$\left|\boldsymbol{\Phi}_{[i,i]}\right| \leq \eta_i, i = 1, 2, \ldots, N, \tag{20e}$$

where P_0 is the transmit power budget of the DFRC-BS, P_{RIS} is the total power consumption budget of the active RIS, and γ_r denotes the minimum SINR threshold at the DFRC-BS receiver with given azimuth angle from the target towards active RIS. Note that the operator $[*]^+$ in the expression of SR is omitted here since we can obtain the optimal value of S as $S = [R_{max}]^+$, where R_{max} denotes the optimal value of Problem (20).

Problem (20) is obviously non-convex due to the complex form and highly coupled variables in the objective function and constraints. It is challenging to directly obtain an optimal solution of the original problem, so AO algorithm is also applied to solve the problem.

III. THE SDR-MM-BASED AO ALGORITHM

In this section, we decouple the original problem into two subproblems, and alternately optimize the transmit beamforming matrix $\mathbf{W}$ and the reflecting coefficient matrix $\boldsymbol{\Phi}$. In particular, we first use the SCA method to tackle the radar SINR constraint, and apply an SDR-MM-based algorithm to iteratively optimize $\mathbf{W}$ and $\boldsymbol{\Phi}$ in the two subproblems.

A. Optimizing $\mathbf{W}$ With Fixed $\boldsymbol{\Phi}$

In this subsection, the transmit beamforming matrix $\mathbf{W}$ at the DFRC-BS is optimized with given reflecting coefficient matrix $\boldsymbol{\Phi}$. Then, the original Problem (20) can be reformulated

as follows:

$$\max_{\mathbf{W}} \quad \ln\left(\frac{1 + \left|\bar{\mathbf{h}}_U^H \mathbf{w}_{M+1}\right|^2}{1 + \left|\bar{\mathbf{h}}_E^H \mathbf{w}_{M+1}\right|^2}\right) \tag{21a}$$

$$\text{s.t.} \quad \xi_R \geq \gamma_r, \tag{21b}$$

$$\text{tr}\left(\mathbf{R}\right) \leq P_0, \tag{21c}$$

$$\text{tr}\left(\mathbf{T}\mathbf{R}\right) \leq \bar{P}_{RIS}, \tag{21d}$$

where $\bar{\mathbf{h}}_U^H, \bar{\mathbf{h}}_E^H, \mathbf{T}$ and $\bar{P}_{RIS}$ are respectively given by

$$\bar{\mathbf{h}}_U^H \triangleq \left(\mathbf{h}_{BU}^H + \mathbf{h}_{RU}^H \boldsymbol{\Phi} \mathbf{H}_{BR}\right) / \sqrt{\sigma_{v_1}^2 \left\|\mathbf{h}_{RU}^H \boldsymbol{\Phi}\right\|_2^2 + \sigma_U^2},$$

$$\bar{\mathbf{h}}_E^H \triangleq \left(\mathbf{h}_{BE}^H + \mathbf{h}_{RE}^H \boldsymbol{\Phi} \mathbf{H}_{BR}\right) / \sqrt{\sigma_{v_1}^2 \left\|\mathbf{h}_{RE}^H \boldsymbol{\Phi}\right\|_2^2 + \sigma_E^2},$$

$$\mathbf{T} \triangleq \mathbf{H}_{BR}^H \boldsymbol{\Phi}^H \boldsymbol{\Phi} \mathbf{H}_{BR} + \mathbf{H}_{BR}^H \boldsymbol{\Phi}^H \mathbf{G}^H \boldsymbol{\Phi} \boldsymbol{\Phi}^H \mathbf{G} \boldsymbol{\Phi} \mathbf{H}_{BR},$$

$$\bar{P}_{RIS} \triangleq P_{RIS} - \left(\sigma_{v_1}^2 + \sigma_{v_2}^2\right) \|\boldsymbol{\Phi}\|_F^2 - \sigma_{v_1}^2 \left\|\boldsymbol{\Phi}^H \mathbf{G} \boldsymbol{\Phi}\right\|_F^2.$$

It is obvious that Problem (21) is still non-convex owing to the forms of objective function (21a) and radar SINR constraint (21b). To tackle this problem, we first apply the SCA method to reformulate constraint (21b) into a more tractable form. By using the following Lemma 1, we can find a convex approximation of ξ_R.

Lemma 1: Given $\mathbf{X}_{(k)}, \mathbf{J}_{(k)}$ as the value of $\mathbf{X}, \mathbf{J}$ in the k-th iteration, we have

$$\text{tr}\left(\mathbf{X}^H \mathbf{J}^{-1} \mathbf{X}\right)$$

$$\geq 2\text{Re}\left(\text{tr}\left(\mathbf{X}_{(k)}^H \mathbf{J}_{(k)}^{-1} \mathbf{X}\right)\right) - \text{tr}\left(\mathbf{J}_{(k)}^{-1} \mathbf{X}_{(k)} \mathbf{X}_{(k)}^H \mathbf{J}_{(k)}^{-1} \mathbf{J}\right). \tag{22}$$

Proof: Please refer to Appendix A. ∎

The lemma provides a lower bound of functions with the form of $\text{tr}(\mathbf{X}^H \mathbf{J}^{-1} \mathbf{X})$. Hence, by letting $\mathbf{X} = \mathbf{A}\mathbf{W}$ in equality (22), ξ_R can be approximated as shown in (23) shown at the bottom of the next page, where $\mathbf{w}_{i(k)}$ denotes the value of $\mathbf{w}_i$ in the k-th iteration, $\mathbf{R}_{(k)} = \mathbf{w}_{i(k)} \mathbf{w}_{i(k)}^H$ and constant $\alpha_1 \triangleq \text{tr}(\mathbf{J}_{(k)}^{-1} \mathbf{A} \mathbf{R}_{(k)} \mathbf{A}^H \mathbf{J}_{(k)}^{-1} \mathbf{N})$. Substituting (23) into (21b), (21b) can be approximated as a more tractable form written as (24) shown at the bottom of the next page.

We next apply the SDR method and let

$$\mathbf{W}_i = \left[\mathbf{w}_i^H, 1\right]^H \left[\mathbf{w}_i^H, 1\right], i = 1, 2, \ldots, M+1. \tag{25}$$

Then, by substituting (23) and (25) into Problem (21) and relaxing the rank-1 constraint, Problem (21) can be reformulated as

$$\max_{\{\mathbf{W}_i\}_{i=1}^{M+1}} \quad C\left(\mathbf{W}_{M+1}\right) \tag{26a}$$

$$\text{s.t.} \quad \sum_{i=1}^{M+1} \text{tr}\left(\mathbf{H}_i \mathbf{W}_i\right) + e_1 \leq 0, \tag{26b}$$

$$\sum_{i=1}^{M+1} \text{tr}\left(\mathbf{W}_i\right) \leq P_0 + M + 1, \tag{26c}$$

$$\sum_{i=1}^{M+1} \mathrm{tr}\left(\bar{\mathbf{T}}\mathbf{W}_i\right) \leq \bar{P}_{\mathrm{RIS}}, \qquad (26\mathrm{d})$$

$$\mathbf{W}_i \succeq \mathbf{0}, \qquad (26\mathrm{e})$$

$$\mathbf{W}_{i[M+1,M+1]} = 1, \qquad (26\mathrm{f})$$

where $\quad e_1 = \alpha_1 + \gamma_{\mathrm{r}}, \quad \bar{\mathbf{T}} = \begin{bmatrix} \mathbf{T} & \mathbf{0}_{M\times 1} \\ \mathbf{0}_{1\times M} & 0 \end{bmatrix}, \quad \mathbf{H}_{\mathrm{U}} = \begin{bmatrix} \bar{\mathbf{h}}_{\mathrm{U}}\bar{\mathbf{h}}_{\mathrm{U}}^{\mathrm{H}} & \mathbf{0}_{M\times 1} \\ \mathbf{0}_{1\times M} & 1 \end{bmatrix}$, $\mathbf{H}_{\mathrm{E}} = \begin{bmatrix} \bar{\mathbf{h}}_{\mathrm{E}}\bar{\mathbf{h}}_{\mathrm{E}}^{\mathrm{H}} & \mathbf{0}_{M\times 1} \\ \mathbf{0}_{1\times M} & 1 \end{bmatrix}$, and

$$\mathbf{H}_i = \begin{bmatrix} \mathbf{B}^{\mathrm{H}}\mathbf{J}_{(k)}^{-1}\mathbf{A}\mathbf{R}_{(k)}\mathbf{A}^{\mathrm{H}}\mathbf{J}_{(k)}^{-1}\mathbf{B} & -\mathbf{A}^{\mathrm{H}}\mathbf{J}_{(k)}^{-1}\mathbf{A}\mathbf{w}_{i(k)} \\ -\mathbf{w}_{i(k)}^{\mathrm{H}}\mathbf{A}^{\mathrm{H}}\mathbf{J}_{(k)}^{-1}\mathbf{A} & 0 \end{bmatrix}. \quad (27)$$

Furthermore, denoting $\mathbf{W}_{\mathrm{c}} = \mathbf{W}_{M+1}$ for simplicity, we have

$$C\left(\mathbf{W}_{\mathrm{c}}\right) \triangleq \ln\left(\mathrm{tr}\left(\mathbf{H}_{\mathrm{U}}\mathbf{W}_{\mathrm{c}}\right)\right) - \ln\left(\mathrm{tr}\left(\mathbf{H}_{\mathrm{E}}\mathbf{W}_{\mathrm{c}}\right)\right). \quad (28)$$

Problem (26) is still non-convex due to the form of the objective function. Hence, the classical iterative approach, i.e., MM algorithm is employed to address this problem. By applying the following Lemma 2, we can obtain a concave surrogate function of (26a) and iteratively solve the problem with the surrogate function.

Lemma 2: For any concave function $f(\mathbf{X})$, we have

$$f\left(\mathbf{X}\right) \leq f\left(\mathbf{X}_{(k)}\right) + \mathrm{tr}\left(\nabla f\left(\mathbf{X}_{(k)}\right)\left(\mathbf{X} - \mathbf{X}_{(k)}\right)\right), \quad (29)$$

where $\mathbf{X}_{(k)}$ is the value of $\mathbf{X}$ in the k-th iteration.

Proof: Please refer to [49]. ∎

The lemma provides a linear lower bound of any concave function. Therefore, with feasible point $\mathbf{W}_{\mathrm{c}(k)}$, the lower bound of the objective function in the $(k+1)$-th iteration can be derived as

$$C\left(\mathbf{W}_{\mathrm{c}}\right) \geq \ln\left(\mathrm{tr}\left(\mathbf{H}_{\mathrm{U}}\mathbf{W}_{\mathrm{c}}\right)\right) - \ln\left(\mathrm{tr}\left(\mathbf{H}_{\mathrm{E}}\mathbf{W}_{\mathrm{c}(k)}\right)\right)$$
$$- \mathrm{tr}\left(\frac{\mathbf{H}_{\mathrm{E}}}{\mathrm{tr}\left(\mathbf{H}_{\mathrm{E}}\mathbf{W}_{\mathrm{c}(k)}\right)}\left(\mathbf{W}_{\mathrm{c}} - \mathbf{W}_{\mathrm{c}(k)}\right)\right)$$
$$\triangleq \tilde{C}\left(\mathbf{W}_{\mathrm{c}}|\mathbf{W}_{\mathrm{c}(k)}\right). \quad (30)$$

It is also simple to verify that $\tilde{C}(\mathbf{W}_{\mathrm{c}}|\mathbf{W}_{\mathrm{c}(k)})$ satisfies the following four conditions [49]:

1) $\tilde{C}(\mathbf{W}_{\mathrm{c}}|\mathbf{W}_{\mathrm{c}(k)})|_{\mathbf{W}_{\mathrm{c}}=\mathbf{W}_{\mathrm{c}(k)}} = C(\mathbf{W}_{\mathrm{c}})|_{\mathbf{W}_{\mathrm{c}}=\mathbf{W}_{\mathrm{c}(k)}}$;
2) $\nabla\tilde{C}(\mathbf{W}_{\mathrm{c}}|\mathbf{W}_{\mathrm{c}(k)})|_{\mathbf{W}_{\mathrm{c}}=\mathbf{W}_{\mathrm{c}(k)}} = \nabla C(\mathbf{W}_{\mathrm{c}})|_{\mathbf{W}_{\mathrm{c}}=\mathbf{W}_{\mathrm{c}(k)}}$;
3) $\tilde{C}(\mathbf{W}_{\mathrm{c}}|\mathbf{W}_{\mathrm{c}(k)}) \leq C(\mathbf{W}_{\mathrm{c}})$;
4) $\tilde{C}(\mathbf{W}_{\mathrm{c}}|\mathbf{W}_{\mathrm{c}(k)})$ is continuous in both $\mathbf{W}_{\mathrm{c}}$ and $\mathbf{W}_{\mathrm{c}(k)}$.

Hence, $\tilde{C}(\mathbf{W}_{\mathrm{c}}|\mathbf{W}_{\mathrm{c}(k)})$ can be considered as a surrogate function of the objective function in Problem (26). By dropping the constant terms in the surrogate function, Problem (26) can be approximated as

$$\max_{\{\mathbf{W}_i\}_{i=1}^{M+1}} \quad \ln\left(\mathrm{tr}\left(\mathbf{H}_{\mathrm{U}}\mathbf{W}_{\mathrm{c}}\right)\right) - \mathrm{tr}\left(\frac{\mathbf{H}_{\mathrm{E}}\mathbf{W}_{\mathrm{c}}}{\mathrm{tr}\left(\mathbf{H}_{\mathrm{E}}\mathbf{W}_{\mathrm{c}(k)}\right)}\right)$$
$$\text{s.t.} \quad (26\mathrm{b}) \sim (26\mathrm{e}), \quad (31\mathrm{a})$$

which is a concave maximization problem and can be directly solved via the MOSEK solver in CVX [50]. Nevertheless, the corresponding beamforming vectors $\mathbf{w}_i$ may not be recovered through the optimal solution of Problem (31) since the rank-1 constraint is omitted. Therefore, the method of eigenvalue decomposition and Gaussian randomization are applied to construct the rank-1 solution.

Furthermore, the convergence of optimizing $\mathbf{W}_i$ is non-decreasing according to the key property of MM algorithm, and we can finally obtain a sub-optimal point of Problem (26). By using the eigenvalue decomposition and Gaussian randomization methods, we can obtain an optimal rank-1 solution $\mathbf{W}_i^{\mathrm{opt}}$, and then the optimal transmit beamforming vectors $\mathbf{w}_i^{\mathrm{opt}}$ can be derived as $(\boldsymbol{\nu}_{\max}(\mathbf{W}_i^{\mathrm{opt}})_{[1:M]})\sqrt{\lambda_{\max}(\mathbf{W}_i^{\mathrm{opt}})}$ and $\mathbf{W}^{\mathrm{opt}} = [\mathbf{w}_1^{\mathrm{opt}}, \mathbf{w}_2^{\mathrm{opt}}, \dots, \mathbf{w}_{M+1}^{\mathrm{opt}}]$, where $\lambda_{\max}(\mathbf{W}_i^{\mathrm{opt}})$ and $\boldsymbol{\nu}_{\max}(\mathbf{W}_i^{\mathrm{opt}})$ denote the largest eigenvalue and its corresponding eigenvector of $\mathbf{W}_i^{\mathrm{opt}}$, respectively.

B. Optimizing $\boldsymbol{\Phi}$ With Fixed $\mathbf{W}$

In this subsection, the reflecting coefficient matrix $\boldsymbol{\Phi}$ at the active RIS is optimized with given beamforming matrix $\mathbf{W}$. Then, Problem (20) can be recast as

$$\max_{\boldsymbol{\Phi}} \quad R_{\mathrm{U}} - R_{\mathrm{E}} \quad (32\mathrm{a})$$

$$\text{s.t.} \quad \xi_{\mathrm{R}} \geq \gamma_{\mathrm{r}}, \quad (32\mathrm{b})$$

$$P_{\mathrm{A}_1} + P_{\mathrm{A}_2} \leq P_{\mathrm{RIS}}, \quad (32\mathrm{c})$$

$$\left|\boldsymbol{\Phi}_{[i,i]}\right| \leq \eta_i, i = 1, 2, \dots, N. \quad (32\mathrm{d})$$

Problem (32) is still non-convex and difficult to handle due to the objective function and the quartic form of $\boldsymbol{\Phi}$ in constraints (32b) and (32c). To this end, we transform the problem into a more tractable form and apply the SDR-MM-based algorithm.

We first denote $\mathbf{v} = [\phi_1, \phi_2, \dots, \phi_N]^{\mathrm{H}} \in \mathbb{C}^{N\times 1}$ for further manipulations. Using vector $\mathbf{v}$, R_i in the objective function can

$$\mathrm{tr}\left(\mathbf{A}\mathbf{R}\mathbf{A}^{\mathrm{H}}\mathbf{J}^{-1}\right) \geq \sum_{i=1}^{M+1} 2\mathrm{Re}\left(\mathbf{w}_{i(k)}^{\mathrm{H}}\mathbf{A}^{\mathrm{H}}\mathbf{J}_{(k)}^{-1}\mathbf{A}\mathbf{w}_i\right) - \sum_{i=1}^{M+1} \mathrm{tr}\left(\mathbf{J}_{(k)}^{-1}\mathbf{A}\mathbf{w}_{i(k)}\mathbf{w}_{i(k)}^{\mathrm{H}}\mathbf{A}^{\mathrm{H}}\mathbf{J}_{(k)}^{-1}\mathbf{J}\right)$$
$$= \sum_{i=1}^{M+1} 2\mathrm{Re}\left(\mathbf{w}_{i(k)}^{\mathrm{H}}\mathbf{A}^{\mathrm{H}}\mathbf{J}_{(k)}^{-1}\mathbf{A}\mathbf{w}_i\right) - \sum_{i=1}^{M+1} \mathrm{tr}\left(\mathbf{J}_{(k)}^{-1}\mathbf{A}\mathbf{R}_{(k)}\mathbf{A}^{\mathrm{H}}\mathbf{J}_{(k)}^{-1}\mathbf{B}\mathbf{w}_i\mathbf{w}_i^{\mathrm{H}}\mathbf{B}^{\mathrm{H}}\right) - \alpha_1. \quad (23)$$

$$\sum_{i=1}^{M+1} \left\{\mathbf{w}_i^{\mathrm{H}}\mathbf{B}^{\mathrm{H}}\mathbf{J}_{(k)}^{-1}\mathbf{A}\mathbf{R}_{(k)}\mathbf{A}^{\mathrm{H}}\mathbf{J}_{(k)}^{-1}\mathbf{B}\mathbf{w}_i - 2\mathrm{Re}\left(\mathbf{w}_{i(k)}^{\mathrm{H}}\mathbf{A}^{\mathrm{H}}\mathbf{J}_{(k)}^{-1}\mathbf{A}\mathbf{w}_i\right)\right\} + \alpha_1 + \gamma_r \leq 0. \quad (24)$$

be expressed as (33) shown at the bottom of this page. We then apply the SDR method, let $\bar{\mathbf{v}} = [\mathbf{v}^{\mathrm{H}}, 1]^{\mathrm{H}}$, $\bar{\mathbf{V}} = \bar{\mathbf{v}}\bar{\mathbf{v}}^{\mathrm{H}}$, and the expression of R_i in (33) can be further reformulated into a more tractable form as $R_i = \ln(\mathrm{tr}(\bar{\mathbf{H}}_{i_1}\bar{\mathbf{V}})) - \ln(\mathrm{tr}(\bar{\mathbf{H}}_{i_2}\bar{\mathbf{V}}))$, where $\bar{\mathbf{H}}_{i_1}$ is given by (34) shown at the bottom of this page, and

$$\bar{\mathbf{H}}_{i_2} = \begin{bmatrix} \mathbf{H}_{i\mathrm{N}} & \mathbf{0}_{N \times 1} \\ \mathbf{0}_{1 \times N} & \sigma_i^2 \end{bmatrix},$$

where $\mathbf{H}_{i\mathrm{N}} = \sigma_{v_1}^2 \mathrm{diag}(\mathbf{h}_{\mathrm{R}i}^{\mathrm{H}})(\mathrm{diag}(\mathbf{h}_{\mathrm{R}i}^{\mathrm{H}}))^{\mathrm{H}}$.

To tackle the quartic form of $\mathbf{\Phi}$ in constraints (32b) and (32c), we first denote $\mathbf{V} = \mathbf{v}\mathbf{v}^{\mathrm{H}}$ and $\hat{\mathbf{v}} = \mathrm{vec}(\mathbf{V})$. By applying Lemma 1, the lower bound of radar SINR in constraint (32b) is given by

$$\mathrm{tr}\left(\mathbf{A}\mathbf{R}\mathbf{A}^{\mathrm{H}}\mathbf{J}^{-1}\right) \geq 2\mathrm{Re}\left(\mathrm{tr}\left(\mathbf{A}\mathbf{R}\mathbf{A}_{(l)}^{\mathrm{H}}\mathbf{J}_{(l)}^{-1}\right)\right)$$
$$- \mathrm{tr}\left(\mathbf{J}_{(l)}^{-1}\mathbf{A}_{(l)}\mathbf{R}\mathbf{A}_{(l)}^{\mathrm{H}}\mathbf{J}_{(l)}^{-1}\mathbf{J}\right), \qquad (35)$$

where $\mathbf{A}_{(l)}, \mathbf{J}_{(l)}$ are the value of $\mathbf{A}, \mathbf{J}$ in the l-th iteration, respectively.

Then, by using the property $\mathrm{tr}(\mathbf{A}^{\mathrm{H}}\mathbf{B}) = (\mathrm{vec}(\mathbf{A}))^{\mathrm{H}}\mathrm{vec}(\mathbf{B})$ [51], the first term on the right hand side of (35) can be reformulated as

$$\mathrm{tr}\left(\mathbf{A}\mathbf{R}\mathbf{A}_{(l)}^{\mathrm{H}}\mathbf{J}_{(l)}^{-1}\right)$$
$$= \mathrm{tr}\left(\mathbf{H}_{\mathrm{BR}}\mathbf{R}\mathbf{A}_{(l)}^{\mathrm{H}}\mathbf{J}_{(l)}^{-1}\mathbf{H}_{\mathrm{BR}}^{\mathrm{H}}\mathbf{\Phi}^{\mathrm{H}}\mathbf{G}\mathbf{\Phi}\right)$$
$$= \left(\mathrm{vec}\left(\mathbf{H}_{\mathrm{BR}}\mathbf{J}_{(l)}^{-1}\mathbf{A}_{(l)}\mathbf{R}\mathbf{H}_{\mathrm{BR}}^{\mathrm{H}}\right)\right)^{\mathrm{H}}\mathrm{vec}\left(\mathbf{\Phi}^{\mathrm{H}}\mathbf{G}\mathbf{\Phi}\right). \quad (36)$$

Furthermore, by using the property $\mathrm{vec}(\mathbf{A}\mathbf{B}\mathbf{C}) = (\mathbf{C}^{\mathrm{T}} \otimes \mathbf{A})\mathrm{vec}(\mathbf{B})$[51], we have

$$\mathrm{vec}\left(\mathbf{\Phi}^{\mathrm{H}}\mathbf{G}\mathbf{\Phi}\right) = \left(\mathbf{\Phi} \otimes \mathbf{\Phi}^*\right)\mathrm{vec}\left(\mathbf{G}\right)$$
$$= \mathrm{diag}\left(\mathrm{vec}\left(\mathbf{G}\right)\right)\hat{\mathbf{v}}, \qquad (37)$$

where the second equation holds since $\mathbf{\Phi} \otimes \mathbf{\Phi}^* = \mathrm{diag}(\hat{\mathbf{v}})$. By using (36) and (37), the first term on the right hand side of (35) can be reformulated as

$$2\mathrm{Re}\left(\mathrm{tr}\left(\mathbf{A}\mathbf{R}\mathbf{A}_{(l)}^{\mathrm{H}}\mathbf{J}_{(l)}^{-1}\right)\right) = 2\mathrm{Re}\left(\mathbf{p}_1^{\mathrm{H}}\hat{\mathbf{v}}\right), \qquad (38)$$

where

$$\mathbf{p}_1^{\mathrm{H}} = \left(\mathrm{vec}\left(\mathbf{H}_{\mathrm{BR}}\mathbf{J}_{(l)}^{-1}\mathbf{A}_{(l)}\mathbf{R}\mathbf{H}_{\mathrm{BR}}^{\mathrm{H}}\right)\right)^{\mathrm{H}}\mathrm{diag}\left(\mathrm{vec}\left(\mathbf{G}\right)\right). \quad (39)$$

By defining the constant matrix $\mathbf{E} = \mathbf{J}_{(l)}^{-1}\mathbf{A}_{(l)}\mathbf{R}\mathbf{A}_{(l)}^{\mathrm{H}}\mathbf{J}_{(l)}^{-1} \succeq \mathbf{0}$ in the l-th iteration, the second term on the right hand side of (35) is transformed into

$$\mathrm{tr}\left(\mathbf{J}_{(l)}^{-1}\mathbf{A}_{(l)}\mathbf{R}\mathbf{A}_{(l)}^{\mathrm{H}}\mathbf{J}_{(l)}^{-1}\mathbf{J}\right)$$

$$= \underbrace{\mathrm{tr}\left(\mathbf{E}\mathbf{H}_{\mathrm{BR}}^{\mathrm{H}}\mathbf{\Phi}\mathbf{\Xi}_1\mathbf{\Phi}^{\mathrm{H}}\mathbf{H}_{\mathrm{BR}}\right)}_{\text{quadratic term}}$$
$$+ \underbrace{2\sigma_{v_1}^2\mathrm{Re}\left(\mathrm{tr}\left(\mathbf{E}\mathbf{H}_{\mathrm{BR}}^{\mathrm{H}}\mathbf{\Phi}^{\mathrm{H}}\mathbf{G}\mathbf{\Phi}\mathbf{\Phi}^{\mathrm{H}}\mathbf{H}_{\mathrm{BR}}\right)\right)}_{\text{cubic term}}$$
$$+ \underbrace{\sigma_{v_1}^2\mathrm{tr}\left(\mathbf{E}\mathbf{H}_{\mathrm{BR}}^{\mathrm{H}}\mathbf{\Phi}^{\mathrm{H}}\mathbf{G}\mathbf{\Phi}\mathbf{\Phi}^{\mathrm{H}}\mathbf{G}^{\mathrm{H}}\mathbf{\Phi}\mathbf{H}_{\mathrm{BR}}\right)}_{\text{quartic term}} + \underbrace{\sigma_{\mathrm{R}}^2\mathrm{tr}\left(\mathbf{E}\right)}_{\text{constant}}, \quad (40)$$

where $\mathbf{\Xi}_1 = (\sigma_{v_1}^2 + \sigma_{v_2}^2)\mathbf{I}_N + \mathbf{H}_{\mathrm{BR}}\mathbf{R}\mathbf{H}_{\mathrm{BR}}^{\mathrm{H}}$. It is worth noting that (40) is a quartic expression with quadratic, cubic and quartic terms with respect to $\mathbf{\Phi}$. To tackle the high-order form of (40), we construct a lower bound of ξ_{R} with a more tractable low-order form. According to the property $\mathrm{tr}(\mathbf{A}\mathbf{B}\mathbf{C}\mathbf{D}) = (\mathrm{vec}(\mathbf{D}^{\mathrm{T}}))^{\mathrm{T}}(\mathbf{C}^{\mathrm{T}} \otimes \mathbf{A})\mathrm{vec}(\mathbf{B})$[51], the quartic term on the left hand side of (40) can be transformed into a quadratic expression of $\hat{\mathbf{v}}$.

$$\sigma_{v_1}^2\mathrm{tr}\left(\mathbf{E}\mathbf{H}_{\mathrm{BR}}^{\mathrm{H}}\mathbf{\Phi}^{\mathrm{H}}\mathbf{G}\mathbf{\Phi}\mathbf{\Phi}^{\mathrm{H}}\mathbf{G}^{\mathrm{H}}\mathbf{\Phi}\mathbf{H}_{\mathrm{BR}}\right)$$
$$= \sigma_{v_1}^2\mathrm{tr}\left(\mathbf{H}_{\mathrm{BR}}\mathbf{E}\mathbf{H}_{\mathrm{BR}}^{\mathrm{H}}\mathbf{\Phi}^{\mathrm{H}}\mathbf{G}\mathbf{\Phi}\mathbf{I}_N\mathbf{\Phi}^{\mathrm{H}}\mathbf{G}^{\mathrm{H}}\mathbf{\Phi}\right)$$
$$= \sigma_{v_1}^2\left(\mathrm{vec}\left(\mathbf{\Phi}^{\mathrm{H}}\mathbf{G}\mathbf{\Phi}\right)\right)^{\mathrm{H}}\left(\mathbf{I}_N \otimes \mathbf{H}_{\mathrm{BR}}\mathbf{E}\mathbf{H}_{\mathrm{BR}}^{\mathrm{H}}\right)\mathrm{vec}\left(\mathbf{\Phi}^{\mathrm{H}}\mathbf{G}\mathbf{\Phi}\right)$$
$$= \hat{\mathbf{v}}^{\mathrm{H}}\mathbf{Q}_1\hat{\mathbf{v}}, \qquad (41)$$

where matrix $\mathbf{Q}_1 = \sigma_{v_1}^2\mathrm{diag}(\mathrm{vec}(\mathbf{G}))^{\mathrm{H}}(\mathbf{I}_N \otimes \mathbf{H}_{\mathrm{BR}}\mathbf{E}\mathbf{H}_{\mathrm{BR}}^{\mathrm{H}})$ $\mathrm{diag}(\mathrm{vec}(\mathbf{G}))$. Then, similar to the method of obtaining (38), the quadratic term on the right hand side of (40) can be further transformed into

$$\mathrm{tr}\left(\mathbf{E}\mathbf{H}_{\mathrm{BR}}^{\mathrm{H}}\mathbf{\Phi}\mathbf{\Xi}_1\mathbf{\Phi}^{\mathrm{H}}\mathbf{H}_{\mathrm{BR}}\right)$$
$$= \left(\mathrm{vec}\left(\mathbf{\Xi}_1\right)\right)^{\mathrm{H}}\mathrm{diag}\left(\mathrm{vec}\left(\mathbf{H}_{\mathrm{BR}}\mathbf{E}\mathbf{H}_{\mathrm{BR}}^{\mathrm{H}}\right)\right)\hat{\mathbf{v}}$$
$$= \mathbf{p}_{2,1}^{\mathrm{H}}\hat{\mathbf{v}}, \qquad (42)$$

where

$$\mathbf{p}_{2,1}^{\mathrm{H}} = \left(\mathrm{vec}\left(\mathbf{\Xi}_1\right)\right)^{\mathrm{H}}\mathrm{diag}\left(\mathrm{vec}\left(\mathbf{H}_{\mathrm{BR}}\mathbf{E}\mathbf{H}_{\mathrm{BR}}^{\mathrm{H}}\right)\right). \qquad (43)$$

Finally, we can obtain a more tractable upper bound of the cubic term on the right hand side of (40) by using the following lemma.

Lemma 3: Given $\mathbf{K}_{(l)}, \mathbf{L}_{(l)}$ as the value of $\mathbf{K}, \mathbf{L}$ in the l-th iteration, we have

$$2\mathrm{Re}\left(\mathrm{tr}\left(\mathbf{K}\mathbf{L}^{\mathrm{H}}\right)\right)$$
$$\leq \frac{\|\mathbf{L}_{(l)}\|_{\mathrm{F}}}{\|\mathbf{K}_{(l)}\|_{\mathrm{F}}}\mathrm{tr}\left(\mathbf{K}\mathbf{K}^{\mathrm{H}}\right) + \frac{\|\mathbf{K}_{(l)}\|_{\mathrm{F}}}{\|\mathbf{L}_{(l)}\|_{\mathrm{F}}}\mathrm{tr}\left(\mathbf{L}\mathbf{L}^{\mathrm{H}}\right).$$

Proof: The above inequality can be obtained through the expansion of $\|\sqrt{\frac{\|\mathbf{L}_{(l)}\|_{\mathrm{F}}}{\|\mathbf{K}_{(l)}\|_{\mathrm{F}}}}\mathbf{K} - \sqrt{\frac{\|\mathbf{K}_{(l)}\|_{\mathrm{F}}}{\|\mathbf{L}_{(l)}\|_{\mathrm{F}}}}\mathbf{L}\|_{\mathrm{F}}^2 \geq 0$. ∎

$$R_i = \ln\left(\left|\left(\mathbf{h}_{\mathrm{B}i}^{\mathrm{H}} + \mathbf{h}_{\mathrm{R}i}^{\mathrm{H}}\mathbf{\Phi}\mathbf{H}_{\mathrm{BR}}\right)\mathbf{w}_{\mathrm{c}}\right|^2 + \sigma_{v_1}^2\left\|\mathbf{h}_{\mathrm{R}i}^{\mathrm{H}}\mathbf{\Phi}\right\|_2^2 + \sigma_i^2\right) - \ln\left(\sigma_{v_1}^2\left\|\mathbf{h}_{\mathrm{R}i}^{\mathrm{H}}\mathbf{\Phi}\right\|_2^2 + \sigma_i^2\right)$$
$$= \ln\left(\left|\left(\mathbf{h}_{\mathrm{B}i}^{\mathrm{H}} + \mathbf{v}^{\mathrm{H}}\mathrm{diag}\left(\mathbf{h}_{\mathrm{R}i}^{\mathrm{H}}\right)\mathbf{H}_{\mathrm{BR}}\right)\mathbf{w}_{\mathrm{c}}\right|^2 + \sigma_{v_1}^2\left\|\mathbf{v}^{\mathrm{H}}\mathrm{diag}\left(\mathbf{h}_{\mathrm{R}i}^{\mathrm{H}}\right)\right\|_2^2 + \sigma_i^2\right) - \ln\left(\sigma_{v_1}^2\left\|\mathbf{v}^{\mathrm{H}}\mathrm{diag}\left(\mathbf{h}_{\mathrm{R}i}^{\mathrm{H}}\right)\right\|_2^2 + \sigma_i^2\right). \quad (33)$$

$$\bar{\mathbf{H}}_{i_1} = \begin{bmatrix} \mathrm{diag}\left(\mathbf{h}_{\mathrm{R}i}^{\mathrm{H}}\right)\mathbf{H}_{\mathrm{BR}}\mathbf{w}_{\mathrm{c}}\mathbf{w}_{\mathrm{c}}^{\mathrm{H}}\mathbf{H}_{\mathrm{BR}}^{\mathrm{H}}\mathrm{diag}\left(\mathbf{h}_{\mathrm{R}i}^{\mathrm{H}}\right)^{\mathrm{H}} + \mathbf{H}_{\mathrm{iN}} & \mathrm{diag}\left(\mathbf{h}_{\mathrm{R}i}^{\mathrm{H}}\right)\mathbf{H}_{\mathrm{BR}}\mathbf{w}_{\mathrm{c}}\mathbf{w}_{\mathrm{c}}^{\mathrm{H}}\mathbf{h}_{\mathrm{B}i} \\ \mathbf{h}_{\mathrm{B}i}^{\mathrm{H}}\mathbf{w}_{\mathrm{c}}\mathbf{w}_{\mathrm{c}}^{\mathrm{H}}\mathbf{H}_{\mathrm{BR}}^{\mathrm{H}}\mathrm{diag}\left(\mathbf{h}_{\mathrm{R}i}^{\mathrm{H}}\right)^{\mathrm{H}} & \sigma_i^2 + \mathbf{w}_{\mathrm{c}}^{\mathrm{H}}\mathbf{h}_{\mathrm{B}i}\mathbf{h}_{\mathrm{B}i}^{\mathrm{H}}\mathbf{w}_{\mathrm{c}} \end{bmatrix}. \qquad (34)$$

Based on Lemma 3, we have

$$2\sigma_{v_1}^2 \mathrm{Re}\left(\mathrm{tr}\left(\mathbf{E}\mathbf{H}_{\mathrm{BR}}^{\mathrm{H}}\boldsymbol{\Phi}^{\mathrm{H}}\mathbf{G}\boldsymbol{\Phi}\boldsymbol{\Phi}^{\mathrm{H}}\mathbf{H}_{\mathrm{BR}}\right)\right)$$

$$\leq \sigma_{v_1}^2\left(\beta^2\left\|\boldsymbol{\Phi}^{\mathrm{H}}\mathbf{H}_{\mathrm{BR}}\mathbf{E}\mathbf{H}_{\mathrm{BR}}^{\mathrm{H}}\right\|_{\mathrm{F}}^2 + \frac{1}{\beta^2}\left\|\boldsymbol{\Phi}^{\mathrm{H}}\mathbf{G}\boldsymbol{\Phi}\right\|_{\mathrm{F}}^2\right)$$

$$= \mathbf{p}_{2,2}^{\mathrm{H}}\hat{\mathbf{v}} + \hat{\mathbf{v}}^{\mathrm{H}}\mathbf{Q}_2\hat{\mathbf{v}}, \tag{44}$$

where $\beta^2 = \|\boldsymbol{\Phi}_{(l)}^{\mathrm{H}}\mathbf{G}\boldsymbol{\Phi}_{(l)}\|_{\mathrm{F}}/\|\boldsymbol{\Phi}_{(l)}^{\mathrm{H}}\mathbf{H}_{\mathrm{BR}}\mathbf{E}\mathbf{H}_{\mathrm{BR}}^{\mathrm{H}}\|_{\mathrm{F}}$ and $\boldsymbol{\Phi}_{(l)}$ denotes the value of $\boldsymbol{\Phi}$ in the l-th iteration, $\mathbf{p}_{2,2}^{\mathrm{H}} = \sigma_{v_1}^2\beta^2(\mathrm{vec}(\mathbf{H}_{\mathrm{BR}}\mathbf{E}\mathbf{H}_{\mathrm{BR}}^{\mathrm{H}}\mathbf{H}_{\mathrm{BR}}\mathbf{E}\mathbf{H}_{\mathrm{BR}}^{\mathrm{H}}))^{\mathrm{H}}\mathrm{diag}(\mathrm{vec}(\mathbf{I}_N))$, and

$$\mathbf{Q}_2 = \frac{\sigma_{v_1}^2}{\beta^2}\left(\mathrm{diag}\left(\mathrm{vec}\left(\mathbf{G}\right)\right)\right)^{\mathrm{H}}\left(\mathrm{diag}\left(\mathrm{vec}\left(\mathbf{G}\right)\right)\right), \tag{45}$$

respectively. Substituting (38), (41), (42) and (44) into (35), a more tractable lower bound of ξ_{R} as a quadratic function of $\hat{\mathbf{v}}$ is given as

$$\xi_{\mathrm{R}} \geq 2\mathrm{Re}\left(\mathbf{p}_1^{\mathrm{H}}\hat{\mathbf{v}}\right) - \mathbf{p}_2^{\mathrm{H}}\hat{\mathbf{v}} - \hat{\mathbf{v}}^{\mathrm{H}}\mathbf{Q}_1\hat{\mathbf{v}} - \hat{\mathbf{v}}^{\mathrm{H}}\mathbf{Q}_2\hat{\mathbf{v}} - \alpha_2, \tag{46}$$

where $\mathbf{p}_2 \triangleq \mathbf{p}_{2,1} + \mathbf{p}_{2,2}$, and $\alpha_2 \triangleq \sigma_{\mathrm{R}}^2\mathrm{tr}(\mathbf{E})$. Since equation $\hat{\mathbf{v}} = \mathrm{vec}(\mathbf{V})$ holds, we can reformulate the right hand side of (46) as a function of $\mathbf{V}$ as

$$2\mathrm{Re}\left(\mathbf{p}_1^{\mathrm{H}}\hat{\mathbf{v}}\right) - \mathbf{p}_2^{\mathrm{H}}\hat{\mathbf{v}} - \hat{\mathbf{v}}^{\mathrm{H}}\mathbf{Q}_1\hat{\mathbf{v}} - \hat{\mathbf{v}}^{\mathrm{H}}\mathbf{Q}_2\hat{\mathbf{v}} - \alpha_2$$

$$= -\mathrm{tr}\left(\mathbf{V}\mathbf{M}_{1,1}\mathbf{V}^{\mathrm{H}}\right) - \mathrm{tr}\left(\mathbf{V}\mathbf{M}_{1,2}\mathbf{V}^{\mathrm{H}}\right)$$

$$+ \mathrm{tr}\left(\mathbf{N}_{1,1}\mathbf{V}\right) + \mathrm{tr}\left(\mathbf{V}^{\mathrm{H}}\mathbf{N}_{1,2}\right) - \alpha_2$$

$$= -\mathrm{tr}\left(\mathbf{V}\mathbf{M}_1\mathbf{V}^{\mathrm{H}}\right) + \mathrm{tr}\left(\mathbf{N}_1\mathbf{V}\right) - \alpha_2, \tag{47}$$

where

$$\mathbf{M}_{1,1} = \mathbf{Q}_{1[1:N,1:N]}, \mathbf{M}_{1,2} = \mathbf{Q}_{2[1:N,1:N]}, \tag{48}$$

$$\mathbf{N}_{1,1}^{\mathrm{H}} = \Sigma\left(\mathbf{p}_1 - \mathbf{p}_2\right), \mathbf{N}_{1,2} = \Sigma\left(\mathbf{p}_1\right), \tag{49}$$

$$\mathbf{M}_1 = \mathbf{M}_{1,1} + \mathbf{M}_{1,2}, \mathbf{N}_1 = \mathbf{N}_{1,1} + \mathbf{N}_{1,2}. \tag{50}$$

The proof of (47), (48) and the positive semi-definiteness of $\mathbf{M}_1$ can be found in Appendix B.

We then transform the expression of the transmit power of the active RIS into the quadratic form of $\mathbf{V}$. In terms of the left hand side of constraint (32c), we have

$$P_{\mathrm{A}_1} + P_{\mathrm{A}_2} = \mathrm{tr}\left(\boldsymbol{\Xi}_2\boldsymbol{\Phi}^{\mathrm{H}}\boldsymbol{\Phi}\right) + \mathrm{tr}\left(\boldsymbol{\Xi}_3\boldsymbol{\Phi}^{\mathrm{H}}\mathbf{G}^{\mathrm{H}}\boldsymbol{\Phi}\boldsymbol{\Phi}^{\mathrm{H}}\mathbf{G}\boldsymbol{\Phi}\right), \tag{51}$$

where $\boldsymbol{\Xi}_2 = \mathbf{H}_{\mathrm{BR}}\mathbf{R}\mathbf{H}_{\mathrm{BR}}^{\mathrm{H}} + (\sigma_{v_1}^2 + \sigma_{v_2}^2)\mathbf{I}_N$, $\boldsymbol{\Xi}_3 = \mathbf{H}_{\mathrm{BR}}\mathbf{R}\mathbf{H}_{\mathrm{BR}}^{\mathrm{H}} + \sigma_{v_1}^2\mathbf{I}_N$, respectively. Then the right hand side of (51) can be reformulated as a function of $\hat{\mathbf{v}}$ as

$$\mathrm{tr}\left(\boldsymbol{\Xi}_2\boldsymbol{\Phi}^{\mathrm{H}}\boldsymbol{\Phi}\right) + \mathrm{tr}\left(\boldsymbol{\Xi}_3\boldsymbol{\Phi}^{\mathrm{H}}\mathbf{G}^{\mathrm{H}}\boldsymbol{\Phi}\boldsymbol{\Phi}^{\mathrm{H}}\mathbf{G}\boldsymbol{\Phi}\right) = \hat{\mathbf{v}}^{\mathrm{H}}\mathbf{Q}_3\hat{\mathbf{v}} + \mathbf{p}_3^{\mathrm{H}}\hat{\mathbf{v}}, \tag{52}$$

where $\mathbf{Q}_3$ and $\mathbf{p}_3$ are respectively given as

$$\mathbf{Q}_3 = \mathrm{diag}\left(\mathrm{vec}\left(\mathbf{G}\right)\right)^{\mathrm{H}}\left(\mathbf{I}_N \otimes \boldsymbol{\Xi}_3\right)\mathrm{diag}\left(\mathrm{vec}\left(\mathbf{G}\right)\right), \tag{53}$$

$$\mathbf{p}_3^{\mathrm{H}} = \left(\mathrm{vec}\left(\boldsymbol{\Xi}_2\right)\right)^{\mathrm{H}}\mathrm{diag}\left(\mathrm{vec}\left(\mathbf{I}_N\right)\right). \tag{54}$$

In addition, the expression of (52) as a function of $\mathbf{V}$ is given as

$$\hat{\mathbf{v}}^{\mathrm{H}}\mathbf{Q}_3\hat{\mathbf{v}} + \mathbf{p}_3^{\mathrm{H}}\hat{\mathbf{v}} = \mathrm{tr}\left(\mathbf{V}\mathbf{M}_2\mathbf{V}^{\mathrm{H}}\right) + \mathrm{tr}\left(\mathbf{N}_2\mathbf{V}\right), \tag{55}$$

where

$$\mathbf{M}_2 = \mathbf{Q}_{3[1:N,1:N]}, \mathbf{N}_2^{\mathrm{H}} = \Sigma\left(\mathbf{p}_3\right). \tag{56}$$

Note that matrix $\mathbf{M}_2$ is also positive semi-definite, and the detailed proof can be found in Appendix B. Finally, the constraint (32d) can be reformulated as $\bar{\mathbf{V}}_{[i,i]} \leq \eta_i^2, i = 1, 2, \ldots, N$, $\bar{\mathbf{V}}_{[N+1,N+1]} = 1$. With the rank-1 constraint relaxed, Problem (32) can be reformulated as

$$\max_{\bar{\mathbf{V}}} \quad R\left(\bar{\mathbf{V}}\right) \tag{57a}$$

$$\mathrm{s.t.} \quad \|\mathbf{V}\mathbf{L}_1\|_{\mathrm{F}}^2 - \mathrm{tr}\left(\mathbf{N}_1\mathbf{V}\right) + e_2 \leq 0, \tag{57b}$$

$$\|\mathbf{V}\mathbf{L}_2\|_{\mathrm{F}}^2 + \mathrm{tr}\left(\mathbf{N}_2\mathbf{V}\right) \leq P_{\mathrm{RIS}}, \tag{57c}$$

$$\bar{\mathbf{V}}_{[i,i]} \leq \eta_i^2, i = 1, 2, \ldots, N, \tag{57d}$$

$$\bar{\mathbf{V}}_{[N+1,N+1]} = 1, \tag{57e}$$

$$\bar{\mathbf{V}} \succeq \mathbf{0}, \tag{57f}$$

where $e_2 = \alpha_2 + \gamma_{\mathrm{r}}$, $\mathbf{L}_i$ are the Cholesky decomposition of positive semi-definite matrices $\mathbf{M}_i$, namely $\mathbf{M}_i = \mathbf{L}_i\mathbf{L}_i^{\mathrm{H}}, i = 1, 2$, and the detailed expression of $R(\bar{\mathbf{V}})$ is shown in (58) shown at the bottom of the next page. Since $\mathbf{V} = \bar{\mathbf{V}}_{[1:N,1:N]}$ is an affine function of optimization variable $\bar{\mathbf{V}}$, it has no influence on the curvature of the constraints. Similar to (26a), we adopt the MM algorithm to tackle the non-convexity of the objective function. By using the first-order Taylor approximation at the given point $\bar{\mathbf{V}}_{(l)}$, the objective function can be transformed into (59) shown at the bottom of the next page. By dropping the constant terms of $\tilde{R}(\bar{\mathbf{V}}|\bar{\mathbf{V}}_{(l)})$, Problem (57) is approximated as

$$\max_{\bar{\mathbf{V}}} \quad \ln\left(\mathrm{tr}\left(\bar{\mathbf{H}}_{\mathrm{U}_1}\bar{\mathbf{V}}\right)\right) - \mathrm{tr}\left(\frac{\bar{\mathbf{H}}_{\mathrm{U}_2}}{\mathrm{tr}\left(\bar{\mathbf{H}}_{\mathrm{U}_2}\bar{\mathbf{V}}_{(l)}\right)}\bar{\mathbf{V}}\right)$$

$$+ \ln\left(\mathrm{tr}\left(\bar{\mathbf{H}}_{\mathrm{E}_2}\bar{\mathbf{V}}\right)\right) - \mathrm{tr}\left(\frac{\bar{\mathbf{H}}_{\mathrm{E}_1}}{\mathrm{tr}\left(\bar{\mathbf{H}}_{\mathrm{E}_1}\bar{\mathbf{V}}_{(l)}\right)}\bar{\mathbf{V}}\right)$$

$$\mathrm{s.t.} \quad (57\mathrm{b}) \sim (57\mathrm{f}), \tag{60a}$$

which is a concave maximization problem and can be solved via the MOSEK solver in CVX toolbox. The convergence of optimizing $\boldsymbol{\Phi}$ is also non-decreasing and we can iteratively obtain the sub-optimal $\bar{\mathbf{V}}$. Similarly, the rank-1 solution of $\bar{\mathbf{V}}$ as $\bar{\mathbf{V}}^{\mathrm{opt}}$ can be recovered by applying the eigenvalue decomposition and Gaussian randomization methods, and the optimal solution $\boldsymbol{\Phi}^{\mathrm{opt}}$ can be obtained through $\bar{\mathbf{V}}^{\mathrm{opt}}$ as $\boldsymbol{\Phi}^{\mathrm{opt}} = \mathrm{diag}((\boldsymbol{\nu}_{\max}(\bar{\mathbf{V}}^{\mathrm{opt}})_{[1:N]})\sqrt{\lambda_{\max}(\bar{\mathbf{V}}^{\mathrm{opt}})})$.

We summarize the detailed procedures of the overall SDR-MM-based AO algorithm to optimize $\mathbf{W}$ and $\boldsymbol{\Phi}$ in Algorithm 1, where $\mathbf{W}_{[0]}$ and $\boldsymbol{\Phi}_{[0]}$ are initialized randomly as the feasible points of the original Problem (20). Note that $\mathbf{W}_{[t]}$ and $\boldsymbol{\Phi}_{[t]}$ denote the values of $\mathbf{W}$ and $\boldsymbol{\Phi}$ in the t-th outer-layer iteration, while $\mathbf{W}_{(k)}$ denotes the value of $\mathbf{W}$ in the k-th inner-layer iteration, and $\boldsymbol{\Phi}_{(l)}$ denotes the value of $\boldsymbol{\Phi}$ in the l-th inner-layer iteration, respectively.

Algorithm 1: SDR-MM-based AO algorithm.

1: Initialize iteration number $t = 0$, the maximum numbers of outer-layer iterations $t^{\max}$ and inner-layer iterations $\tau_1^{\max}, \tau_2^{\max}$. Initialize $\mathbf{W}_{[0]}$ and $\mathbf{\Phi}_{[0]}$.
2: **Repeat:**
3:     Let $k = 0$.
4:     **Repeat:**
5:        Calculate $\mathbf{W}_{i(k+1)}$ according to (31).
6:        Recover the rank-1 solution by eigenvalue decomposition and Gaussian randomization.
7:        Let $k = k + 1$.
8:     **Until** *Convergence* **or** $k = \tau_1^{\max}$.
9:     Let $\mathbf{W}_{[t]} = \mathbf{W}_{(k)}$, and $l = 0$.
10:    **Repeat:**
11:       Calculate $\mathbf{\Phi}_{(l+1)}$ according to (60).
12:       Recover the rank-1 solution by eigenvalue decomposition and Gaussian randomization.
13:       Let $l = l + 1$.
14:    **Until** *Convergence* **or** $l = \tau_2^{\max}$.
15:    Let $\mathbf{\Phi}_{[t]} = \mathbf{\Phi}_{(l)}$, and $t = t + 1$.
16: **Until** *Convergence* **or** $t = t^{\max}$.

C. Algorithm Analysis

1) Convergence Analysis: According to the aforementioned analysis, the convergence of the MM algorithm is non-decreasing. Since our variables $\mathbf{W}$ and $\mathbf{\Phi}$ are bounded by constraints, the convergence of the proposed SDR-MM-based AO algorithm is also non-decreasing and a sub-optimal point of our original problem can be obtained when the SDR-MM-based AO algorithm converges.

2) Complexity Analysis: The computational complexity of solving Problem (31) and (60) mainly lies in the interior point method, which is given by [52]

$$\mathcal{O}\left(\left(\sum_{j=1}^{J} k_j + 2m \right)^{\frac{1}{2}} n \left(n^2 + \sum_{j=1}^{J} \left(k_j^2 + k_j^3 \right) + n \sum_{i=1}^{m} a_i^2 \right) \right),$$

where n denotes the number of variables, J denotes the number of linear matrix inequality (LMI) constraints, k_j denotes the size of the j-th LMI constraint, m denotes the number of second-order cone (SOC) constraints, and a_i is the size of the i-th SOC constraint.

We first analyze the complexity of solving Problem (31) and (60) with CVX. Problem (31) contains $J_1 = (M + 4)$ LMI constraints of size $k_1 = (M + 1)$, and the number of variables is $n_1 = (M + 1)^3$. Ignoring the constant value, the approximate computation complexity of Problem (31) is given as $o_1 = \mathcal{O}((J_1 k_1)^{1/2} n_1 (n_1^2 + n_1 J_1 k_1^2 + J_1 k_1^3))$. Similarly, the approximate computational complexity of solving Problem (60) with $J_2 = 2, k_2 = (N + 1), n_2 = (N + 1)^2, m_2 = 2, a_2 = (N + 1)^2$ is given by $o_2 = \mathcal{O}((J_2 k_2 + 2m_2)^{1/2} n_2 (n_2^2 + n_2 J_2 k_2^2 + J_2 k_2^3 + n_2 m_2 a_2))$. Furthermore, to obtain the computational complexity of Algorithm 1, let us define t_{AO} as the number of iterations of the AO algorithm, t_1 as the number of iterations of beamforming matrix optimization, and t_2 as the number of iterations of reflecting coefficient matrix optimization. Hence, the overall computational complexity of the proposed algorithm is given as $t_{\mathrm{AO}}(t_1 o_1 + t_2 o_2)$.

IV. SIMULATION RESULTS

In this section, simulation results are provided to illustrate the advantage of integrating an active RIS into the DFRC system for enhancing the dual-functional performance. Each simulation result in this section is obtained as the average of more than 100 independent channel samples.

A. Simulation Setup

1) Communication Channels: According to the aforementioned system model, the location of the active RIS is designed carefully with few obstacles in the wireless environment, while the DFRC-BS may be located in a relatively crowded area. Thus, without loss of generality, channels $\mathbf{H}_{\mathrm{BR}}$, $\mathbf{h}_{\mathrm{RU}}$, and $\mathbf{h}_{\mathrm{RE}}$ are modeled as Rician fading, and channels $\mathbf{h}_{\mathrm{BU}}$ and $\mathbf{h}_{\mathrm{BE}}$ are modeled as Rayleigh fading, respectively. The small-scale fading model of Rician channel is given as

$$\bar{\mathbf{H}} = \sqrt{\frac{1}{\kappa + 1}} \bar{\mathbf{H}}_{\mathrm{NLoS}} + \sqrt{\frac{\kappa}{\kappa + 1}} \bar{\mathbf{H}}_{\mathrm{LoS}}, \tag{61}$$

where κ denotes the Rician factor, $\bar{\mathbf{H}}_{\mathrm{NLoS}}$ and $\bar{\mathbf{H}}_{\mathrm{LoS}}$ denote the NLoS and LoS channel component between two devices, respectively. The NLoS component $\bar{\mathbf{H}}_{\mathrm{NLoS}}$ follows Rayleigh fading, and the LoS component $\bar{\mathbf{H}}_{\mathrm{LoS}}$ can be expressed as $\mathbf{a}_2(\theta_2)\mathbf{a}_1^{\mathrm{H}}(\theta_1)$, where

$$\mathbf{a}_1(\theta_1) = \left[1, e^{j2\pi \frac{d_1}{\lambda} \sin\theta_1}, \ldots, e^{j2\pi \frac{d_1}{\lambda}(D_t - 1)\sin\theta_1} \right]^{\mathrm{H}}, \tag{62}$$

$$R\left(\bar{\mathbf{V}}\right) = \ln\left(\mathrm{tr}\left(\bar{\mathbf{H}}_{\mathrm{U1}}\bar{\mathbf{V}}\right)\right) - \ln\left(\mathrm{tr}\left(\bar{\mathbf{H}}_{\mathrm{U2}}\bar{\mathbf{V}}\right)\right) - \ln\left(\mathrm{tr}\left(\bar{\mathbf{H}}_{\mathrm{E1}}\bar{\mathbf{V}}\right)\right) + \ln\left(\mathrm{tr}\left(\bar{\mathbf{H}}_{\mathrm{E2}}\bar{\mathbf{V}}\right)\right). \tag{58}$$

$$\tilde{R}\left(\bar{\mathbf{V}}|\bar{\mathbf{V}}_{(l)}\right) = \ln\left(\mathrm{tr}\left(\bar{\mathbf{H}}_{\mathrm{U1}}\bar{\mathbf{V}}\right)\right) - \ln\left(\mathrm{tr}\left(\bar{\mathbf{H}}_{\mathrm{U2}}\bar{\mathbf{V}}_{(l)}\right)\right) - \mathrm{tr}\left(\frac{\bar{\mathbf{H}}_{\mathrm{U2}}}{\mathrm{tr}\left(\bar{\mathbf{H}}_{\mathrm{U2}}\bar{\mathbf{V}}_{(l)}\right)}\left(\bar{\mathbf{V}} - \bar{\mathbf{V}}_{(l)}\right)\right)$$

$$+ \ln\left(\mathrm{tr}\left(\bar{\mathbf{H}}_{\mathrm{E2}}\bar{\mathbf{V}}\right)\right) - \ln\left(\mathrm{tr}\left(\bar{\mathbf{H}}_{\mathrm{E1}}\bar{\mathbf{V}}_{(l)}\right)\right) - \mathrm{tr}\left(\frac{\bar{\mathbf{H}}_{\mathrm{E1}}}{\mathrm{tr}\left(\bar{\mathbf{H}}_{\mathrm{E1}}\bar{\mathbf{V}}_{(l)}\right)}\left(\bar{\mathbf{V}} - \bar{\mathbf{V}}_{(l)}\right)\right). \tag{59}$$

$$\mathbf{a}_2\left(\theta_2\right)=\left[1, e^{j2\pi\frac{d_2}{\lambda}\sin\theta_2}, \ldots, e^{j2\pi\frac{d_2}{\lambda}(D_r-1)\sin\theta_2}\right]^{\mathrm{H}}. \quad (63)$$

Parameters D_r and D_t denote the number of antennas/elements at the side of the receiver and transmitter, the angles θ_1 and θ_2 denote the AoD and the angle of arrival (AoA), and d_1, d_2 denote the intervals between adjacent antennas/elements, respectively.

The large-scale path loss in dB is modeled as

$$\mathrm{PL}=\mathrm{PL}_0-10\alpha\lg\left(\frac{d}{d_0}\right), \quad (64)$$

where $\mathrm{PL}_0 = -30$ dB is the path loss at the reference distance $d_0 = 1$ m, d is the link distance, and α denotes the large-scale path loss exponent.

2) Sensing Response Channel: To evaluate the fading nature of the target response channel, radar range equation is referenced to model the path loss coefficient γ in matrix $\mathbf{G}$. By assuming that the target can be considered as a single scatter object, and the wireless sensing environment can be viewed as free space, the received radar echo power is given as

$$P_{\mathrm{r}}=P_{\mathrm{t}}\frac{G^2\lambda^2\Delta}{(4\pi)^3 R^4}, \quad (65)$$

where P_t denotes the transmit power, G denotes the array gain at the radar, λ denotes the wavelength and Δ denotes the radar cross section (RCS) of the sensing target, respectively. Since the direct link between the DFRC-BS and the target is obstructed, the active RIS can also be regarded as a monostatic MIMO radar, and the complex path loss coefficient can be modeled as

$$\gamma=\sqrt{\frac{\lambda^2\Delta}{(4\pi)^3 R^4}}, \quad (66)$$

where the RCS of the sensing target is set as $\Delta = 1\mathrm{m}^2$[53].

3) Parameters Setup: Unless otherwise stated, the simulation parameters are set as follows: Carrier frequency of $f = 2.7$ GHz, channel bandwidth of $B = 10$ MHz, power density of thermal noise at the legitimate user, eavesdropper, radar receiver and active RIS of $\sigma^2/B = -174$ dBm/Hz[28], number of transmit antennas of $M = 4$, number of reflecting elements of active RIS of $N = 12$, maximum power budget of the BS of $P_0 = 30$ dBm, maximum power budget of the active RIS of $P_{\mathrm{RIS}} = 17$ dBm, the threshold of radar echo SINR of $\gamma_{\mathrm{r}} = -60$ dB, Rician factor of $\kappa = 3$, and the large-scale path loss exponents of Rayleigh and Rician channels are set to $\alpha_1 = 3.5$ and $\alpha_2 = 2.2$, respectively. For simplicity, the normalized intervals d/λ are set to 0.5. For Algorithm 1, the target accuracy of convergence is set as $\epsilon = 10^{-3}$ for both the inner-layer and the outer-layer iterations. Finally, the geometrical model is arranged as shown in Fig. 2.

B. Baseline Schemes

In order to illustrate the superiority of the active RIS-assisted scheme in enhancing the dual-function of the DFRC system, we compare the proposed scheme with the following benchmarks:

1) *No RIS No Sensing:* To compare the SR gain obtained by the active and passive RISs, we implement a scheme
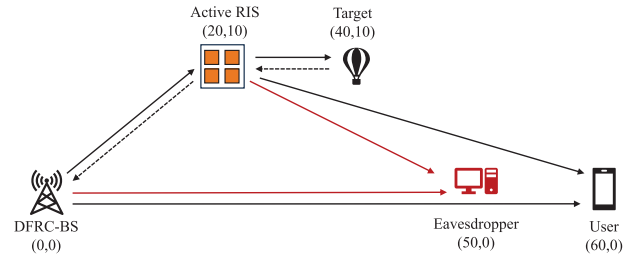
Fig. 2. Simulation system setup.

with no RIS as a lower bound of SR performance with the sensing function ignored.

2) *Passive RIS:* The passive RIS-related algorithm is almost the same as the original SDR-MM-based AO algorithm. Considering the property of the passive RIS, the terms generated by the amplified thermal noise and constraint (20d) are dropped, and constraint (20e) is reformulated as unit-modulus constraint.

For the fairness of our comparison, the total power consumption is considered. The total power budgets of the three schemes are respectively given as

$$Q^{\mathrm{act}}=P_0^{\mathrm{act}}+P_{\mathrm{RIS}}+N^{\mathrm{act}}\left(P_{\mathrm{SW}}+P_{\mathrm{DC}}\right), \quad (67)$$

$$Q^{\mathrm{pas}}=P_0^{\mathrm{pas}}+N^{\mathrm{pas}}P_{\mathrm{SW}}, \quad (68)$$

$$Q^{\mathrm{NRNS}}=P_0^{\mathrm{NRNS}}, \quad (69)$$

where $Q^{\mathrm{act}}, Q^{\mathrm{pas}}$ and Q^{NRNS} are the total power of the schemes "Active RIS", "Passive RIS" and "No RIS No Sensing", and $P_0^{\mathrm{act}}, P_0^{\mathrm{pas}}$ and P_0^{NRNS} are the transmit power at the BS of the schemes "Active RIS", "Passive RIS" and "No RIS No Sensing", respectively. The scalar $P_{\mathrm{SW}} = -5$ dBm denotes the power consumption in phase control of each element of the RISs, and $P_{\mathrm{DC}} = -10$ dBm denotes the direct-current (DC) power consumption of each active RIS element. After accounting for the power budget at the active RIS, the remaining power is allocated to the BS for the schemes "Passive RIS" and "No RIS No Sensing".

C. Convergence Behavior of the Algorithm

In this subsection, the convergence behavior of our algorithm is shown in Fig. 3. As depicted, the SDR-MM-based AO algorithm converges within 20 outer-layer iterations with different parameter settings, which indicates the good convergence behavior of our algorithm in different scenarios. In addition, it is shown that the secrecy performance can be enhanced by increasing the number of antennas, the number of RIS elements and the maximum amplitude gain of the active RIS as expected. Furthermore, it is depicted that there is a slight SR gain in the "Without Sensing" scheme compared with the default scheme, which indicates that there is a trade-off between the communication and sensing performance of the secure DFRC system.

D. Sensing Function of the Proposed Scheme

The sensing function of the proposed scheme is investigated in this subsection. The cumulative distribution functions (CDF)
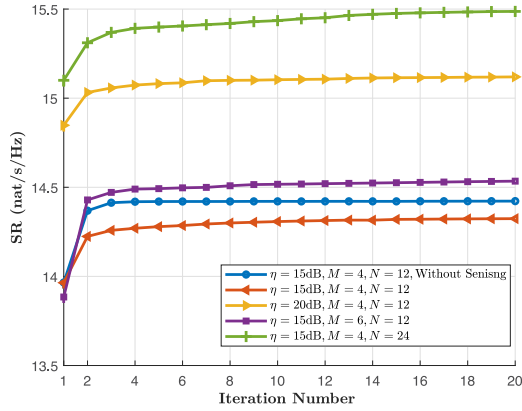
Fig. 3.   Convergence behavior of the proposed algorithm.
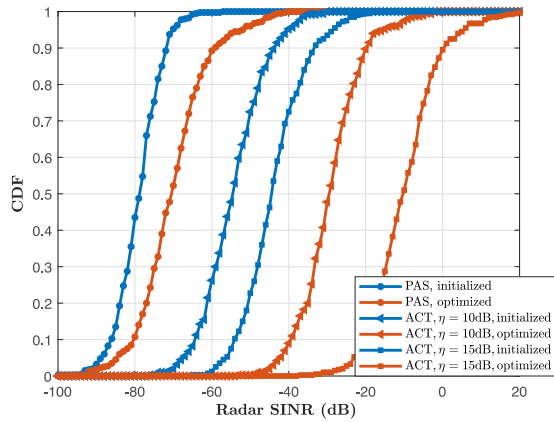
Fig. 4.   CDF of radar echo SINR.

Fig. 5.   System SR versus the maximum transmit power.
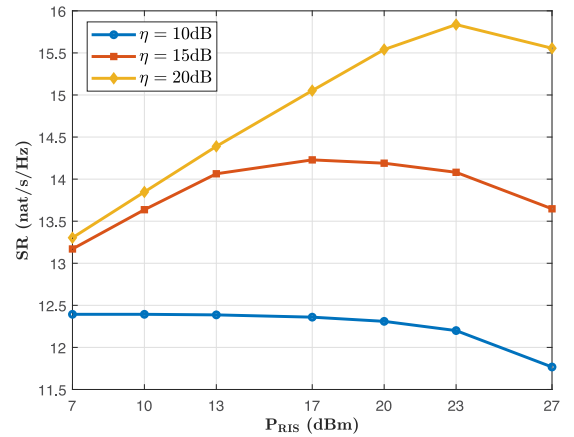
Fig. 6.   System SR versus power allocation at the active RIS.

of radar echo SINR are shown in Fig. 4, where the CDFs corresponding to the initialized values of $\mathbf{W}$ and $\boldsymbol{\Phi}$ are labeled as "initialized" and those corresponding to the optimized values are labeled as "optimized", respectively. The threshold of radar echo SINR γ_r is set as -100 dB to ensure the feasibility of the passive RIS-assisted scheme. In addition, for the fairness of our comparison between the initialized and optimized schemes, the initialized beamforming matrix $\mathbf{W}$ satisfies $\mathrm{tr}(\mathbf{W}\mathbf{W}^H) = P_0$, and each diagonal element of the initialized reflecting coefficient matrix $\boldsymbol{\Phi}$ is with the amplitude of 0.95η and random phase shift.

As depicted in Fig. 4, the radar SINR of the active RIS-assisted schemes significantly exceed those of the passive RIS-assisted those. Specifically, the mean SINR of the active RIS with $\eta = 15$ dB exceeds that of the passive RIS by approximately 60 dB. In addition, although the radar SINR is in constraint (20b) instead of the objective function, the sensing performance of the RIS-assisted systems is still enhanced with the SDR-MM-based algorithm. In addition, it is worth noting that the sensing performance gain of the active RIS-assisted schemes also prevail over their passive counterparts. For instance, the SINR gain of the active RIS with $\eta = 15$ dB is approximately 35 dB, which greatly exceeds 10 dB of the passive RIS-assisted scheme. Therefore, we can conclude that the active RIS outperforms its passive counterpart in terms of sensing performance.

E. Secrecy Rate Versus the Maximum Transmit Power

The impact of the maximum transmit power at the BS and active RIS is illustrated in Fig. 6. It is worth noting that the total power budget is actually not the same among different schemes in Fig. 6, but we can still observe some phenomena from the result.

As shown in Fig. 6, it is obvious that there is an approximate logarithmic relationship between the SR and P_0. In addition, there is only a slight gain of the passive RIS-assisted system owing to the severe path loss of the RIS reflecting channel. In contrast, the active RIS-assisted schemes achieve much better performance in terms of secrecy rate. Specifically, when $P_0 = 30$ dBm, the passive RIS obtains an SR gain of only 0.38 nat/s/Hz, in other words 3.63%, while the active RIS with $\eta = 10/15$ dB obtains a gain of 2.04/4.02 nat/s/Hz, in other words 19.5%/38.4% respectively with an extra power consumption of 17 dBm. In addition, when $P_0 = 30$ dBm and $P_{\mathrm{RIS}} = 17$ dBm, the total power budget of the active RIS with $\eta = 15$ dB is 30.28 dBm < 31 dBm. Nevertheless, the corresponding SR performance still exceeds that of the passive RIS-assisted scheme with $P_0 = 31$ dBm by 1.81 nat/s/Hz. This verifies the ability of the active RIS in combating the "multiplicative fading" effect,

and indicates the advantage of deploying an active RIS over a passive RIS in terms of secure wireless communication.

Furthermore, the transmit power budget at the active RIS also has an impact on the achievable SR. As illustrated in Fig. 6, the SR with $P_{\text{RIS}} = 17$ dBm and $\eta = 20$ dB merely obtains a slight increase compared with the $P_{\text{RIS}} = 17$ dBm, $\eta = 15$ dB scheme and finally reaches its limit, while the SR with $P_{\text{RIS}} = 27$ dBm, $\eta = 20$ dB obviously exceeds the aforementioned counterparts. This is owing to the fact that the maximum transmit power at the active RIS is decisive for the maximum power received at the legitimate user. In particular, when the active RIS is operating at the maximum transmit power, it is difficult to increase the received power at the legitimate user by increasing the transmit power at the DFRC-BS, and thereby posing a limit on the achievable SR. Therefore, we can conclude that the maximum transmit power at the active RIS determines the achievable upper bound of SR with the same P_0 at the DFRC-BS, and the relationship between secrecy performance and power allocation between the DFRC-BS and the active RIS is further explored in the following subsection.

F. Secrecy Rate Versus Power Allocation

Fig. 5 illustrates the relationship between the secrecy performance and the power allocation of the system. Note that the total power budget in this subsection is in correspondence with the default setup, where the total power budget is set as 30.28 dBm.

As depicted in Fig. 5, it is beneficial to allocate adequate power to the active RIS for better secrecy performance, and the critical factor of the power allocation is the maximum amplification gain of the active RIS. Specifically, when η of the active RIS is relatively high, the SR performance experiences an initial increase but then declines with the increase of P_{RIS}. This is owing to the fact that the operating amplification gain of the elements are rising with the increase of the transmit power budget at the active RIS. Nevertheless, when most of the elements are approximately operating at the maximum amplitude gain η, extra power allocation will not be effective for improving the SR performance, while the SR will decline owing to the decrease in transmit power at the DFRC-BS. Furthermore, since more power is required for active RIS elements with larger amplitude gain to reach their limit, the power budget at the active RIS corresponding to the maximum secrecy performance also increases with the maximum amplitude gain η.

G. Secrecy Rate Versus the Number of RIS Elements

Fig. 7 illustrates the relationship between SR and the number of reflecting elements. As expected, the secure communication performance ascends along with the increase in the number of RIS elements. In addition, the active RIS-assisted schemes significantly prevail over the passive RIS-assisted scheme with the same power budget and the equal number of RIS elements. The diminishing return law and the impact of P_{RIS} are also obvious in relevant schemes. Specifically, the SR performance gap between the $\eta = 15$ dB, $P_{\text{RIS}} = 17$ dBm is approximately 1 nat/s/Hz with $N = 12$, which reduces to 0.18 nat/s/Hz with $N = 36$ owing to the limited power at the active RIS. Furthermore, the SR gain obtained by increasing the number of elements from 12
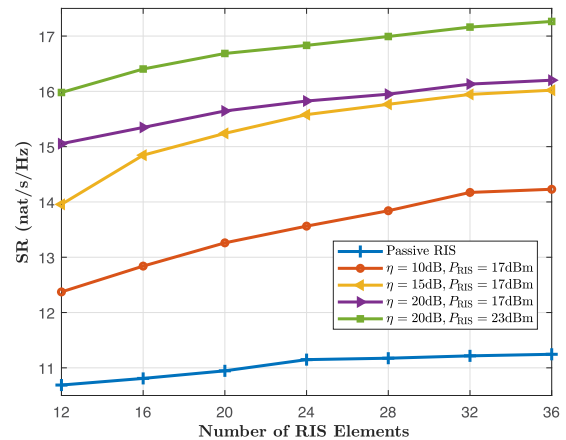
Fig. 7. System SR versus the number of elements N.
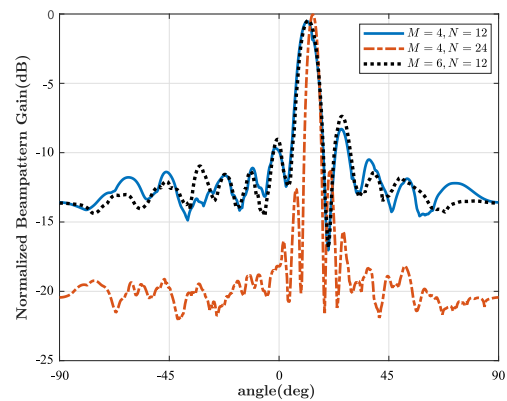
Fig. 8. Normalized beampattern gain.

to 36 can exceed that of increasing the maximum amplitude gain by approximately 5 dB with proper power allocation between the DFRC-BS and the active RIS.

H. Beampattern of the Proposed Scheme

As is mentioned above, since the direct link between the DFRC-BS and the sensing target is obstructed, it is reasonable to regard the active RIS as a monostatic MIMO radar. Hence, we denote the beampattern at the active RIS as

$$P\left(\theta\right) = \mathbb{E}\left\{\left|\mathbf{a}^{\text{H}}\left(\theta\right)\mathbf{\Phi}\mathbf{H}_{\text{BR}}\mathbf{x}\right|^2\right\}$$
$$= \mathbf{a}^{\text{H}}\left(\theta\right)\mathbf{\Phi}\mathbf{H}_{\text{BR}}\mathbf{R}\mathbf{H}_{\text{BR}}^{\text{H}}\mathbf{\Phi}^{\text{H}}\mathbf{a}\left(\theta\right), \quad (70)$$

where θ denotes the AoD at the active RIS. We investigate the normalized beampattern gain of the proposed scheme in Fig. 8.

It is depicted that the center of the main lobe is located at the AoD of the legitimate user instead of the target, which is due to the fact that the objective function is the SR of the system instead of the radar SINR. In addition, the normalized beampattern shows a trough at the AoD of the eavesdropper and a side lobe at the AoD of the target, respectively. Furthermore, it is worth noting that the width of the main lobe is obviously reduced and the side lobes are effectively suppressed by increasing the number of RIS elements, while more antennas at the BS cannot lead to better directivity of the sensing function.

V. CONCLUSION

In this paper, we studied the dual-function of an active RIS-assisted DFRC system with the presence of active eavesdropping, where the radar sensing performance is evaluated with the four-hop radar echo. In particular, we aimed at solving the SR maximization problem by jointly optimizing the beamforming matrix at the DFRC-BS and the reflecting coefficient matrix at the active RIS, subject to the radar echo SINR constraint and the transmit power consumption constraints. An SDR-MM-based AO algorithm was proposed to tackle the complicated non-convex optimization problem. Specifically, we first utilized the SCA method to transform the radar SINR constraint into a more tractable form, then applied the SDR and MM algorithms to iteratively solve the problem. Our simulation results validated that the amplification function of the active RIS not only enhances the performance in physical layer security, but also observably overcomes the "multiplicative fading" effect of the four-hop sensing channel. Furthermore, the active RIS prevails over traditional passive RIS in both secure communication as well as radar sensing with the same transmit power budget.

APPENDIX A
PROOF OF LEMMA 1

Since it is readily verified that function $g(\mathbf{X}, \mathbf{X}^*, \mathbf{J}) = \mathrm{tr}(\mathbf{X}^\mathrm{H}\mathbf{J}^{-1}\mathbf{X})$ is jointly convex of $\{\mathbf{X}, \mathbf{J}\}$, we will obtain a lower bound of $g(\mathbf{X}, \mathbf{X}^*, \mathbf{J})$ by linearizing it at feasible point $\{\mathbf{X}_{(k)}, \mathbf{J}_{(k)}\}$ as

$$
g(\mathbf{X}, \mathbf{X}^*, \mathbf{J}) \geq g(\mathbf{X}_{(k)}, \mathbf{X}^*_{(k)}, \mathbf{J}_{(k)})
$$
$$
+ \mathrm{tr}\left(\left(\frac{\partial g}{\partial \mathbf{X}} \bigg|_{\mathbf{X}=\mathbf{X}_{(k)}} \right)^\mathrm{T} (\mathbf{X} - \mathbf{X}_{(k)}) \right)
$$
$$
+ \mathrm{tr}\left(\left(\frac{\partial g}{\partial \mathbf{X}^*} \bigg|_{\mathbf{X}^*=\mathbf{X}^*_{(k)}} \right)^\mathrm{T} (\mathbf{X}^* - \mathbf{X}^*_{(k)}) \right)
$$
$$
+ \mathrm{tr}\left(\left(\frac{\partial g}{\partial \mathbf{J}} \bigg|_{\mathbf{J}=\mathbf{J}_{(k)}} \right)^\mathrm{T} (\mathbf{J} - \mathbf{J}_{(k)}) \right), \quad (71)
$$

where the first-order derivatives can be obtained in [51] as

$$
\frac{\partial g}{\partial \mathbf{X}} = \left(\mathbf{J}^{-1}\right)^\mathrm{T} \mathbf{X}^*, \tag{72}
$$

$$
\frac{\partial g}{\partial \mathbf{X}^*} = \mathbf{J}^{-1}\mathbf{X}, \tag{73}
$$

$$
\frac{\partial g}{\partial \mathbf{J}} = \left(\mathbf{J}^{-1}\mathbf{X}\mathbf{X}^\mathrm{H}\mathbf{J}^{-1}\right)^\mathrm{T}. \tag{74}
$$

Hence, we can obtain the lower bound of $g(\mathbf{X}, \mathbf{X}^*, \mathbf{J})$ by substituting the above derivatives into (71) as

$$
\mathrm{tr}\left(\mathbf{X}^\mathrm{H}\mathbf{J}^{-1}\mathbf{X}\right)
$$
$$
\geq 2\mathrm{Re}\left(\mathrm{tr}\left(\mathbf{X}^\mathrm{H}_{(k)}\mathbf{J}^{-1}_{(k)}\mathbf{X} \right) \right) - \mathrm{tr}\left(\mathbf{J}^{-1}_{(k)}\mathbf{X}_{(k)}\mathbf{X}^\mathrm{H}_{(k)}\mathbf{J}^{-1}_{(k)}\mathbf{J} \right),
$$
$$
\tag{75}
$$

which is actually inequality (22) and the proof is completed.

APPENDIX B
PROOF OF EQUATION (47), (48) AND (56)

Note that $\mathbf{Q}_1 = \sigma^2_{v_1}\mathrm{diag}(\mathrm{vec}(\mathbf{G}))^\mathrm{H}(\mathbf{I}_N \otimes \mathbf{H}_{\mathrm{BR}}\mathbf{E}\mathbf{H}^\mathrm{H}_{\mathrm{BR}})$ $\mathrm{diag}(\mathrm{vec}(\mathbf{G}))$, $\mathbf{M}_{1,1} = \mathbf{Q}_{[1:N,1:N]}$, and we will derive that $\hat{\mathbf{v}}^\mathrm{H}\mathbf{Q}_1\hat{\mathbf{v}} = \mathrm{tr}(\mathbf{V}\mathbf{M}_{1,1}\mathbf{V}^\mathrm{H})$ as follows.

Let us define $\mathbf{G}_0 = \gamma\mathrm{diag}(\mathbf{a}(\theta))$, and we have

$$
\mathrm{diag}\left(\mathrm{vec}\left(\mathbf{G}\right)\right) = \begin{bmatrix} \lambda_1\mathbf{G}_0 & \mathbf{0} & \cdots & \mathbf{0} \\ \mathbf{0} & \lambda_2\mathbf{G}_0 & \cdots & \mathbf{0} \\ \cdots & \cdots & \cdots & \cdots \\ \mathbf{0} & \mathbf{0} & \cdots & \lambda_N\mathbf{G}_0 \end{bmatrix}, \tag{76}
$$

where $\lambda_i, i = 1, 2, \ldots, N$ denotes the i-th element of $\mathbf{a}^\mathrm{H}(\theta)$. In addition, let $\mathbf{F} = \mathbf{H}_{\mathrm{BR}}\mathbf{E}\mathbf{H}^\mathrm{H}_{\mathrm{BR}} \succeq \mathbf{0}$, and the expression of $\mathbf{Q}_1$ can be further transformed into

$$
\sigma^2_{v_1}\mathrm{diag}\left(\mathrm{vec}\left(\mathbf{G}\right)\right)^\mathrm{H}\left(\mathbf{I}_N \otimes \mathbf{F}\right)\mathrm{diag}\left(\mathrm{vec}\left(\mathbf{G}\right)\right)
$$

$$
= \sigma^2_{v_1}\begin{bmatrix} |\lambda_1|^2\mathbf{G}^\mathrm{H}_0\mathbf{F}\mathbf{G}_0 & \mathbf{0} & \cdots & \mathbf{0} \\ \mathbf{0} & |\lambda_2|^2\mathbf{G}^\mathrm{H}_0\mathbf{F}\mathbf{G}_0 & \cdots & \mathbf{0} \\ \cdots & \cdots & \cdots & \cdots \\ \mathbf{0} & \mathbf{0} & \cdots & |\lambda_N|^2\mathbf{G}^\mathrm{H}_0\mathbf{F}\mathbf{G}_0 \end{bmatrix}
$$

$$
= \sigma^2_{v_1}\begin{bmatrix} \mathbf{G}^\mathrm{H}_0\mathbf{F}\mathbf{G}_0 & \mathbf{0} & \cdots & \mathbf{0} \\ \mathbf{0} & \mathbf{G}^\mathrm{H}_0\mathbf{F}\mathbf{G}_0 & \cdots & \mathbf{0} \\ \cdots & \cdots & \cdots & \cdots \\ \mathbf{0} & \mathbf{0} & \cdots & \mathbf{G}^\mathrm{H}_0\mathbf{F}\mathbf{G}_0 \end{bmatrix}. \tag{77}
$$

Since $\mathbf{G}^\mathrm{H}_0\mathbf{F}\mathbf{G}_0 \succeq \mathbf{0}$, it can be easily derived that $\mathbf{Q}_1$ is also positive semi-definite. We then derive that $\mathbf{M}_{1,1} = \mathbf{Q}_{[1:N,1:N]} = \mathbf{G}^\mathrm{H}_0\mathbf{F}\mathbf{G}_0$ satisfies $\hat{\mathbf{v}}^\mathrm{H}\mathbf{Q}_1\hat{\mathbf{v}} = \mathrm{tr}(\mathbf{V}\mathbf{M}_{1,1}\mathbf{V}^\mathrm{H})$. By applying equation $\mathrm{tr}(\mathbf{A}\mathbf{B}\mathbf{C}\mathbf{D}) = (\mathrm{vec}(\mathbf{D}^\mathrm{T}))^\mathrm{T}(\mathbf{C}^\mathrm{T} \otimes \mathbf{A})\mathrm{vec}(\mathbf{B})$, and letting $\mathbf{A} = \mathbf{G}^\mathrm{H}_0\mathbf{F}\mathbf{G}_0, \mathbf{B} = \mathbf{D} = \mathbf{V}, \mathbf{C} = \mathbf{I}_N$, we have

$$
\hat{\mathbf{v}}^\mathrm{H}\mathbf{Q}_1\hat{\mathbf{v}} = (\mathrm{vec}\left(\mathbf{V}\right))^\mathrm{H}\left(\mathbf{I}_N \otimes \left(\mathbf{G}^\mathrm{H}_0\mathbf{F}\mathbf{G}_0\right)\right)\mathrm{vec}\left(\mathbf{V}\right)
$$
$$
= \left(\mathrm{vec}\left(\mathbf{V}^\mathrm{T}\right)\right)^\mathrm{T}\left(\mathbf{I}_N \otimes \left(\mathbf{G}^\mathrm{H}_0\mathbf{F}\mathbf{G}_0\right)\right)\mathrm{vec}\left(\mathbf{V}\right)
$$
$$
= \mathrm{tr}\left(\mathbf{G}^\mathrm{H}_0\mathbf{F}\mathbf{G}_0\mathbf{V}^\mathrm{H}\mathbf{V}\right)
$$
$$
= \mathrm{tr}\left(\mathbf{V}\mathbf{M}_{1,1}\mathbf{V}^\mathrm{H}\right). \tag{78}
$$

Note that $\mathbf{M}_{1,1} = \mathbf{G}^\mathrm{H}_0\mathbf{F}\mathbf{G}_0$ is also semi-definite. In addition, positive semi-definiteness of $\mathbf{Q}_2, \mathbf{Q}_3$ and the method of obtaining $\mathbf{M}_{1,2}, \mathbf{M}_2$ form $\mathbf{Q}_2, \mathbf{Q}_3$ can be derived likewise. Hence, the proof of (47), (48) and (56) is completed.

REFERENCES

[1] L. Zheng, M. Lops, Y. C. Eldar, and X. Wang, "Radar and communication coexistence: An overview: A review of recent methods," *IEEE Signal Process. Mag.*, vol. 36, no. 5, pp. 85–99, Sep. 2019.

[2] Y. He, Y. Cai, H. Mao, and G. Yu, "RIS-assisted communication radar coexistence: Joint beamforming design and analysis," *IEEE J. Sel. Areas Commun.*, vol. 40, no. 7, pp. 2131–2145, Jul. 2022.

[3] F. Liu, L. Zhou, C. Masouros, A. Li, W. Luo, and A. Petropulu, "Toward dual-functional radar-communication systems: Optimal waveform design," *IEEE Trans. Signal Process.*, vol. 66, no. 16, pp. 4264–4279, Aug. 2018.

[4] F. Liu, L. Zhou, C. Masouros, A. Lit, W. Luo, and A. Petropulu, "Dual-functional cellular and radar transmission: Beyond coexistence," in *Proc. IEEE 19th Int. Workshop Signal Process. Adv. Wireless Commun.*, Jun. 2018, pp. 1–5.

[5] A. Hassanien, M. G. Amin, Y. D. Zhang, and F. Ahmad, "Dual-function radar-communications: Information embedding using sidelobe control and waveform diversity," *IEEE Trans. Signal Process.*, vol. 64, no. 8, pp. 2168–2181, Apr. 2016.

[6] A. Deligiannis, A. Daniyan, S. Lambotharan, and J. A. Chambers, "Secrecy rate optimizations for MIMO communication radar," *IEEE Trans. Aerosp. Electron. Syst.*, vol. 54, no. 5, pp. 2481–2492, Oct. 2018.

[7] B. K. Chalise and M. G. Amin, "Performance tradeoff in a unified system of communications and passive radar: A secrecy capacity approach," *Digit. Signal Process.*, vol. 82, pp. 282–293, Nov. 2018.

[8] N. Su, F. Liu, and C. Masouros, "Secure radar-communication systems with malicious targets: Integrating radar, communications and jamming functionalities," *IEEE Trans. Wireless Commun.*, vol. 20, no. 1, pp. 83–95, Jan. 2021.

[9] N. Su, F. Liu, Z. Wei, Y.-F. Liu, and C. Masouros, "Secure dual-functional radar-communication transmission: Exploiting interference for resilience against target eavesdropping," *IEEE Trans. Wireless Commun.*, vol. 21, no. 9, pp. 7238–7252, Sep. 2022.

[10] J. Chen, Y.-C. Liang, Y. Pei, and H. Guo, "Intelligent reflecting surface: A programmable wireless environment for physical layer security," *IEEE Access*, vol. 7, pp. 82599–82612, 2019.

[11] Z. Chu, W. Hao, P. Xiao, and J. Shi, "Intelligent reflecting surface aided multi-antenna secure transmission," *IEEE Wireless Commun. Lett.*, vol. 9, no. 1, pp. 108–112, Jan. 2020.

[12] M. Cui, G. Zhang, and R. Zhang, "Secure wireless communication via intelligent reflecting surface," *IEEE Wireless Commun. Lett.*, vol. 8, no. 5, pp. 1410–1414, Oct. 2019.

[13] X. Yu, D. Xu, D. W. K. Ng, and R. Schober, "IRS-assisted green communication systems: Provable convergence and robust optimization," *IEEE Trans. Commun.*, vol. 69, no. 9, pp. 6313–6329, Sep. 2021.

[14] D. Xu, X. Yu, Y. Sun, D. W. K. Ng, and R. Schober, "Resource allocation for secure IRS-assisted multiuser MISO systems," in *Proc. IEEE Globecom Workshops*, 2019, pp. 1–6.

[15] G. Zhou, C. Pan, H. Ren, K. Wang, and Z. Peng, "Secure wireless communication in RIS-aided MISO system with hardware impairments," *IEEE Wireless Commun. Lett.*, vol. 10, no. 6, pp. 1309–1313, Jun. 2021.

[16] Z.-M. Jiang et al., "Intelligent reflecting surface aided dual-function radar and communication system," *IEEE Syst. J.*, vol. 16, no. 1, pp. 475–486, Mar. 2022.

[17] X. Song, D. Zhao, H. Hua, T. X. Han, X. Yang, and J. Xu, "Joint transmit and reflective beamforming for IRS-assisted integrated sensing and communication," in *Proc. IEEE Wireless Commun. Netw. Conf.*, Apr. 2022, pp. 189–194.

[18] R. P. Sankar, S. P. Chepuri, and Y. C. Eldar, "Beamforming in integrated sensing and communication systems with reconfigurable intelligent surfaces," *IEEE Trans. Wireless Commun.*, vol. 23, no. 5, pp. 4017–4031, May 2024.

[19] M. Hua, Q. Wu, C. He, S. Ma, and W. Chen, "Joint active and passive beamforming design for IRS-aided radar-communication," *IEEE Trans. Wireless Commun.*, vol. 22, no. 4, pp. 2278–2294, Apr. 2023.

[20] M. Hua, Q. Wu, W. Chen, O. A. Dobre, and A. L. Swindlehurst, "Secure intelligent reflecting surface-aided integrated sensing and communication," *IEEE Trans. Wireless Commun.*, vol. 23, no. 1, pp. 575–591, Jan. 2024.

[21] Z. Zhu, M. Gong, G. Sun, M. De, F. Liu, and Y. Liu, "AI-enabled STAR-RIS aided MISO ISAC secure communications," 2024, *arXiv:2402.16413*.

[22] Z. Li et al., "Intelligent reflective surface assisted integrated sensing and wireless power transfer," *IEEE Trans. Intell. Transp. Syst.*, vol. 25, no. 10, pp. 15122–15127, 2024.

[23] Z. Zhang et al., "Active RIS vs. passive RIS: Which will prevail in 6G?," *IEEE Trans. Commun.*, vol. 71, no. 3, pp. 1707–1725, Mar. 2023.

[24] Q. Wu, S. Zhang, B. Zheng, C. You, and R. Zhang, "Intelligent reflecting surface-aided wireless communications: A tutorial," *IEEE Trans. Commun.*, vol. 69, no. 5, pp. 3313–3351, May 2021.

[25] C. Pan et al., "An overview of signal processing techniques for RIS/IRS-aided wireless systems," *IEEE J. Sel. Topics Signal Process.*, vol. 16, no. 5, pp. 883–917, Aug. 2022.

[26] C. Hu, L. Dai, S. Han, and X. Wang, "Two-timescale channel estimation for reconfigurable intelligent surface aided wireless communications," *IEEE Trans. Commun.*, vol. 69, no. 11, pp. 7736–7747, Nov. 2021.

[27] C. Pan et al., "Multicell MIMO communications relying on intelligent reflecting surfaces," *IEEE Trans. Wireless Commun.*, vol. 19, no. 8, pp. 5218–5233, Aug. 2020.

[28] K. Zhi, C. Pan, H. Ren, K. K. Chai, and M. Elkashlan, "Active RIS versus passive RIS: Which is superior with the same power budget?," *IEEE Commun. Lett.*, vol. 26, no. 5, pp. 1150–1154, May 2022.

[29] Z. Zhu et al., "Active reconfigurable intelligent surface enhanced internet of medical things," *IEEE J. Biomed. Health Inform.*, vol. 28, no. 7, pp. 3831–3840, Jul. 2024.

[30] L. Dong, H.-M. Wang, and J. Bai, "Active reconfigurable intelligent surface aided secure transmission," *IEEE Trans. Veh. Technol.*, vol. 71, no. 2, pp. 2181–2186, Feb. 2022.

[31] W. Lv, J. Bai, Q. Yan, and H. M. Wang, "RIS-assisted green secure communications: Active RIS or passive RIS?," *IEEE Wireless Commun. Lett.*, vol. 12, no. 2, pp. 237–241, Feb. 2023.

[32] Y. Guo, Y. Liu, Q. Wu, Q. Shi, and Y. Zhao, "Enhanced secure communication via novel double-faced active RIS," *IEEE Trans. Commun.*, vol. 71, no. 6, pp. 3497–3512, Jun. 2023.

[33] G. Mylonopoulos, C. D'Andrea, and S. Buzzi, "Active reconfigurable intelligent surfaces for user localization in mmwave MIMO systems," in *Proc. IEEE 23rd Int. Workshop Signal Process. Adv. Wireless Commun.*, 2022, pp. 1–5.

[34] Y. Zhang, J. Chen, C. Zhong, H. Peng, and W. Lu, "Active IRS-assisted integrated sensing and communication in C-RAN," *IEEE Wireless Commun. Lett.*, vol. 12, no. 3, pp. 411–415, Mar. 2023.

[35] Z. Yu et al., "Active RIS-aided ISAC systems: Beamforming design and performance analysis," *IEEE Trans. Commun.*, vol. 72, no. 3, pp. 1578–1595, Mar. 2024.

[36] G. Sun, H. Shi, B. Shang, and W. Hao, "Secure transmission for active RIS-assisted THz ISAC systems with delay alignment modulation," *IEEE Commun. Lett.*, vol. 28, no. 5, pp. 1019–1023, May 2024.

[37] A. A. Salem, M. H. Ismail, and A. S. Ibrahim, "Active reconfigurable intelligent surface-assisted MISO integrated sensing and communication systems for secure operation," *IEEE Trans. Veh. Technol.*, vol. 72, no. 4, pp. 4919–4931, Apr. 2023.

[38] X. Liu, T. Huang, N. Shlezinger, Y. Liu, J. Zhou, and Y. C. Eldar, "Joint transmit beamforming for multiuser MIMO communications and MIMO radar," *IEEE Trans. Signal Process.*, vol. 68, pp. 3929–3944, 2020.

[39] Z. Wang, L. Liu, and S. Cui, "Channel estimation for intelligent reflecting surface assisted multiuser communications: Framework, algorithms, and analysis," *IEEE Trans. Wireless Commun.*, vol. 19, no. 10, pp. 6607–6620, Oct. 2020.

[40] X. Guan, Q. Wu, and R. Zhang, "Anchor-assisted channel estimation for intelligent reflecting surface aided multiuser communication," *IEEE Trans. Wireless Commun.*, vol. 21, no. 6, pp. 3764–3778, Jun. 2022.

[41] G. Zhou, C. Pan, H. Ren, P. Popovski, and A. L. Swindlehurst, "Channel estimation for RIS-aided multiuser millimeter-wave systems," *IEEE Trans. Signal Process.*, vol. 70, pp. 1478–1492, 2022.

[42] J. Zhu, R. Schober, and V. K. Bhargava, "Secure transmission in multicell massive MIMO systems," *IEEE Trans. Wireless Commun.*, vol. 13, no. 9, pp. 4766–4781, Sep. 2014.

[43] S. Sun, W. U. Bajwa, and A. P. Petropulu, "MIMO-MC radar: A. MIMO radar approach based on matrix completion," *IEEE Trans. Aerosp. Electron. Syst.*, vol. 51, no. 3, pp. 1839–1852, Jul. 2015.

[44] S. Sun and A. P. Petropulu, "Waveform design for MIMO radars with matrix completion," *IEEE J. Sel. Topics Signal Process.*, vol. 9, no. 8, pp. 1400–1414, Dec. 2015.

[45] H. Hua, J. Xu, and T. X. Han, "Transmit beamforming optimization for integrated sensing and communication," in *Proc. IEEE Glob. Commun. Conf.*, Dec. 2021, pp. 1–6.

[46] F. Liu et al., "Integrated sensing and communications: Toward dual-functional wireless networks for 6G and beyond," *IEEE J. Sel. Areas Commun.*, vol. 40, no. 6, pp. 1728–1767, Jun. 2022.

[47] B. Li and A. Petropulu, "MIMO radar and communication spectrum sharing with clutter mitigation," in *Proc. IEEE Radar Conf.*, May 2016, pp. 1–6.

[48] L. Zheng, M. Lops, X. Wang, and E. Grossi, "Joint design of overlaid communication systems and pulsed radars," *IEEE Trans. Signal Process.*, vol. 66, no. 1, pp. 139–154, Jan. 2018.

[49] Y. Sun, P. Babu, and D. P. Palomar, "Majorization-minimization algorithms in signal processing, communications, and machine learning," *IEEE Trans. Signal Process.*, vol. 65, no. 3, pp. 794–816, Feb. 2017.

[50] M. Grant and S. Boyd, "CVX: Matlab software for disciplined convex programming, version 2.1," 2014.

[51] X.-D. Zhang, *Matrix Analysis and Applications*. Cambridge, U.K.: Cambridge Univ. Press, 2017.

[52] G. Zhou, C. Pan, H. Ren, K. Wang, and A. Nallanathan, "A framework of robust transmission design for IRS-aided MISO communications with imperfect cascaded channels," *IEEE Trans. Signal Process.*, vol. 68, pp. 5092–5106, 2020.

[53] M. A. Richards, *Fundamentals of Radar Signal Processing*. New York, NY, USA: McGraw-Hill Education, 2014.

Yang Zhang received the B.E. degree from the Harbin Institute of Technology, Harbin, China, in 2023. He is currently working toward the M.E. degree with the School of Information Science and Engineering, Southeast University, Nanjing, China. His research interests include reconfigurable intelligent surfaces (RIS), array signal processing, near-field communications, and localization.

Hong Ren (Member, IEEE) received the B.S. degree in electrical engineering from Southwest Jiaotong University, Chengdu, China, in 2011, and the M.S. and Ph.D. degrees in electrical engineering from Southeast University, Nanjing, China, in 2014 and 2018, respectively. From 2016 to 2018, she was a Visiting Student with the School of Electronics and Computer Science, University of Southampton, Southampton, U.K. From 2018 to 2020, she was a Postdoctoral Scholar with the Queen Mary University of London, London, U.K. She is currently an Associate Professor with Southeast University. Her research interests include the areas of communication and signal processing, cooperative ISAC, machine learning, and URLLC. She was the recipient of the 2024 lEEE Communications Society Fred WEllersick Prize and the 2022 lEEE Communications Society Leonard G. AbrahamPrize.

Cunhua Pan (Senior Member, IEEE) is currently a Full Professor with Southeast University, Nanjing, China. He has authored or coauthored more than 200 IEEE journal papers. His papers got more than 16,000 Google Scholar citations with H-index of 63. He is also a Clarivate Highly Cited Researcher. His research interests mainly include reconfigurable intelligent surfaces (RIS), AI for Wireless, and near field communications and sensing. He is/was the Editor of IEEE TRANSACTION ON COMMUNICATIONS, IEEE TRANSACTIONS ON VEHICULAR TECHNOLOGY, IEEE WIRELESS COMMUNICATION LETTERS, IEEE COMMUNICATIONS LETTERS, and IEEE ACCESS. He is also the Guest Editor of IEEE JOURNAL ON SELECTED AREAS IN COMMUNICATIONS on the special issue on xURLLC in 6G: Next Generation Ultra-Reliable and Low-Latency Communications. He is the Leading Guest Editor of IEEE JOURNAL OF SELECTED TOPICS IN SIGNAL PROCESSING (JSTSP) Special Issue on Advanced Signal Processing for Reconfigurable Intelligent Surface-aided 6G Networks, *IEEE Vehicular Technology Magazine* on the special issue on Backscatter and Reconfigurable Intelligent Surface Empowered Wireless Communications in 6G, IEEE OPEN JOURNAL OF VEHICULAR TECHNOLOGY on the special issue of Reconfigurable Intelligent Surface Empowered Wireless Communications in 6G and Beyond, and IEEE TRANSACTIONS ON GREEN COMMUNICATIONS AND NETWORKING Special Issue on Design of Green Near-Field Wireless Communication Networks. He was the recipient of the IEEE ComSoc Leonard G. Abraham Prize in 2022, IEEE ComSoc Asia-Pacific Outstanding Young Researcher Award, 2022 and IEEE ComSoc Fred W. Ellersick Prize in 2024.

Boshi Wang received the B.S. degree in 2023 from the School of Information Science and Engineering, Southeast University, Nanjing, China, where he is currently working toward the master's degree. His research focuses on reconfigurable intelligent surfaces (RIS).

Zhiyuan Yu received the B.S. degree in 2023 from the School of Information Science and Engineering, Southeast University, Nanjing, China, where he is currently working toward the master's degree. His research interests include reconfigurable intelligent surfaces (RIS), integrated sensing, and communication (ISAC).

Ruisong Weng received the B.E. degree from Software Institute, Nanjing University, Nanjing, China, in 2020, and the M.E. degree from the College of Information, Mechanical and Electrical Engineering, Shanghai Normal University, Shanghai, China, in 2023. He is currently working toward the Ph.D. degree with the School of Information Science and Engineering, Southeast University, Nanjing. His research interests include reconfigurable intelligent surface (RIS), channel estimation, and signal processing.

Tuo Wu received the B. Eng. degree in telecommunication engineering from South China Normal University, Guangzhou, China, in 2017, and the M.S. degree in wireless radio physics from Sun Yat-Sen University, Guangzhou, in 2021, and the Ph.D. degree from the School of Electronic Engineering and Computer Science, Queen Mary University of London, London, U.K., in 2024. He is currently a Postdoctoral Researcher with the School of Electrical and Electronic Engineering, Nanyang Technological University, Singapore. His research interests include reconfigurable intelligent surface, wireless localization, fluid antenna systems, and near-field communications.

Yongchao He received the B.S. degree from the School of Communication and Information Engineering, Nanjing University of Posts and Telecommunications, Nanjing, China, in 2023. He is currently working toward the the master's degree with Southeast University, Nanjing. His research interests include reconfigurable smart surfaces (RIS) and 5G new radio (NR) link-level simulation.